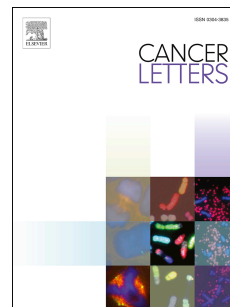


# Journal Pre-proof



*ETS-related gene (ERG)* undermines genome stability in mouse prostate progenitors via Gsk3 $\beta$  dependent Nkx3.1 degradation

Marco Lorenzoni, Dario De Felice, Giulia Beccaceci, Giorgia Di Donato, Veronica Foletto, Sacha Genovesi, Arianna Bertossi, Francesco Cambuli, Francesca Lorenzin, Aurora Savino, Lidia A Valle, Alessia Cimadamore, Rodolfo Montironi, Veronica Weber, Francesco Giuseppe Carbone, Mattia Barbareschi, Francesca Demichelis, Alessandro Romanel, Valeria Poli, Giannino Del Sal, Marianna Kruithof-de Julio, Marco Gaspari, Alessandro Alaimo, Andrea Lunardi

PII: S0304-3835(22)00087-8

DOI: <https://doi.org/10.1016/j.canlet.2022.215612>

Reference: CAN 215612

To appear in: *Cancer Letters*

Received Date: 21 November 2021

Revised Date: 23 February 2022

Accepted Date: 25 February 2022

Please cite this article as: M. Lorenzoni, D. De Felice, G. Beccaceci, G. Di Donato, V. Foletto, S. Genovesi, A. Bertossi, F. Cambuli, F. Lorenzin, A. Savino, L. A Valle, A. Cimadamore, R. Montironi, V. Weber, F.G. Carbone, M. Barbareschi, F. Demichelis, A. Romanel, V. Poli, G. Del Sal, M.K.-d. Julio, M. Gaspari, A. Alaimo, A. Lunardi, *ETS-related gene (ERG)* undermines genome stability in mouse prostate progenitors via Gsk3 $\beta$  dependent Nkx3.1 degradation, *Cancer Letters* (2022), doi: <https://doi.org/10.1016/j.canlet.2022.215612>.

This is a PDF file of an article that has undergone enhancements after acceptance, such as the addition of a cover page and metadata, and formatting for readability, but it is not yet the definitive version of record. This version will undergo additional copyediting, typesetting and review before it is published in its final form, but we are providing this version to give early visibility of the article. Please note that, during the production process, errors may be discovered which could affect the content, and all legal disclaimers that apply to the journal pertain.

© 2022 Published by Elsevier B.V.

## ***Authors' Contributions***

**Conception and design:** M. Lorenzoni, D. De Felice, M. Gaspari, A. Alaimo, A. Lunardi.

**Development of methodology:** M. Lorenzoni, D. De Felice, F. Cambuli, M. Gaspari, A. Alaimo, A. Lunardi.

**Acquisition of data:** M. Lorenzoni, D. De Felice, A. Alaimo, S. Genovesi, G. Beccaceci, G. Di Donato, V. Foletto, F. Lorenzin, V. Weber, A. Savino, A. Cimadamore, R. Montironi, F.G. Carbone, M. Barbareschi, L. Avalle, A. Bertossi, A. Romanel, M. Gaspari.

**Analysis and interpretation of data:** M. Lorenzoni, D. De Felice, A. G. Beccaceci, G. Di Donato, V. Foletto, A. Savino, L. Avalle, A. Bertossi, F. Cambuli, F. Lorenzin, S. Genovesi, F.G. Carbone, M. Barbareschi, A. Cimadamore, R. Montironi, F. Demichelis, V. Poli, A. Romanel, G. Del Sal, M. Kruithof-de Julio, M. Gaspari, A. Alaimo, A. Lunardi.

**Writing, review, and/or revision of the manuscript:** M. Lorenzoni, D. De Felice, F. Demichelis, V. Poli, M. Kruithof-de Julio, G. Del Sal, M. Gaspari, A. Alaimo, A. Lunardi.

**Administrative, technical, or material support:** S. Genovesi, M. Lorenzoni, A. Cimadamore, D. De Felice, V. Foletto, V. Weber, A. Alaimo.

**Study supervision:** A. Lunardi.

# ***ETS-related gene (ERG) undermines genome stability in mouse prostate progenitors via Gsk3 $\beta$ dependent Nkx3.1 degradation***

Marco Lorenzoni<sup>1,¶,\*</sup>, Dario De Felice<sup>1,\*</sup>, Giulia Beccaceci<sup>1</sup>, Giorgia Di Donato<sup>1</sup>, Veronica Foletto<sup>1</sup>, Sacha Genovesi<sup>1</sup>, Arianna Bertossi<sup>1</sup>, Francesco Cambuli<sup>1,#</sup>, Francesca Lorenzin<sup>1</sup>, Aurora Savino<sup>2</sup>, Lidia Avalor<sup>2</sup>, Alessia Cimadamore<sup>3</sup>, Rodolfo Montironi<sup>4</sup>, Veronica Weber<sup>5</sup>, Francesco Giuseppe Carbone<sup>5</sup>, Mattia Barbareschi<sup>5</sup>, Francesca Demichelis<sup>1</sup>, Alessandro Romanel<sup>1</sup>, Valeria Poli<sup>2</sup>, Giannino Del Sal<sup>6</sup>, Marianna Kruithof-de Julio<sup>7,8,9,10</sup>, Marco Gaspari<sup>11,§</sup>, Alessandro Alaimo<sup>1,§</sup>, Andrea Lunardi<sup>1,§</sup>.

<sup>1</sup>Department of Cellular, Computational and Integrative Biology-CIBIO, University of Trento, Trento, Italy

<sup>2</sup>Department of Molecular Biotechnology and Health Sciences, University of Torino, Torino, Italy

<sup>3</sup>Pathological Anatomy, School of Medicine, United Hospitals, Polytechnic University of the Marche Region, Ancona, Italy.

<sup>4</sup>Molecular Medicine and Cell Therapy Foundation, Polytechnic University of the Marche Region, Via Tronto, 10, Ancona, Italy

<sup>5</sup>Unit of Surgical Pathology, Santa Chiara Hospital, Trento, Italy

<sup>6</sup>University of Trieste Department Life Sciences, ICGEB-Area Science Park Trieste, IFOM-Milan, Italy

<sup>7</sup>Urology Research Laboratory, Department for BioMedical Research DBMR, University of Bern, Bern, Switzerland.

<sup>8</sup>Translational Organoid Resource CORE, Department for BioMedical Research, University of Bern, Bern, Switzerland.

<sup>9</sup>Bern Center for Precision Medicine, Inselspital, University Hospital of Bern, Bern, Switzerland.

<sup>10</sup>Department of Urology, Inselspital, University Hospital of Bern, Bern, Switzerland.

<sup>11</sup>Research Centre for Advanced Biochemistry and Molecular Biology, Department of Experimental and Clinical Medicine, Magna Graecia University of Catanzaro, Catanzaro, Italy

Present address: <sup>¶</sup> Cellular Immunology Unit, IRCCS Ospedale San Raffaele, Milan, Italy; <sup>#</sup> Molecular Pharmacology Program, Sloan Kettering Institute, Memorial Sloan Kettering Cancer Center, New York, NY, USA

<sup>§</sup>Corresponding Author: Marco Gaspari [gaspari@unicz.it](mailto:gaspari@unicz.it), Alessandro Alaimo [alessandro.alaimo@unitn.it](mailto:alessandro.alaimo@unitn.it), Andrea Lunardi [andrea.lunardi@unitn.it](mailto:andrea.lunardi@unitn.it)

\* equally contributed

Running title: ERG functions in preneoplastic prostate epithelium

Key words: Prostate, Organoids, ERG, Wnt, Nkx3.1, Egf

39 **Abstract**

40 21q22.2-3 deletion is the most common copy number alteration in prostate cancer (PCa). The  
41 genomic rearrangement results in the androgen-dependent *de novo* expression of *ETS-related gene*  
42 (*ERG*) in prostate cancer cells, a condition promoting tumor progression to advanced stages of the  
43 disease.

44 Interestingly, *ERG* expression characterizes 5-30% of tumor precursor lesions – High Grade  
45 Prostatic Intraepithelial Neoplasia (HGPIN) - where its role remains unclear.

46 Here, by combining organoids technology with Click-chemistry coupled Mass Spectrometry, we  
47 demonstrate a prominent role of *ERG* in remodeling the protein secretome of prostate progenitors.  
48 Functionally, by lowering autocrine Wnt-4 signaling, *ERG* represses canonical Wnt pathway in  
49 prostate progenitors, and, in turn, promotes the accumulation of DNA double strand breaks via  
50 Gsk3 $\beta$ -dependent degradation of the tumor suppressor Nkx3.1. On the other hand, by shaping  
51 extracellular paracrine signals, *ERG* strengthens the pro-oxidative transcriptional signature of  
52 inflammatory macrophages, which we demonstrate to infiltrate pre-malignant *ERG* positive prostate  
53 lesions.

54 These findings highlight previously unrecognized functions of *ERG* in undermining adult prostate  
55 progenitor niche through cell autonomous and non-autonomous mechanisms. Overall, by supporting  
56 the survival and proliferation of prostate progenitors in the absence of growth stimuli and promoting  
57 the accumulation of DNA damage through destabilization of Nkx3.1, *ERG* could orchestrate the  
58 prelude to neoplastic transformation.

59

60

61

62

63

64

65

## 66 **Introduction**

67 Prostate Cancer (PCa) is one of the most commonly diagnosed cancer in men [1]. In addition to  
68 aging, other risk factors are ethnicity (African American > Caucasian > Asian), family history  
69 (hereditary gene mutations of *BRCA2*), and lifestyle [2–5].

70 PCa is a slow-growing tumor commonly considered the natural progression of proliferative lesions  
71 characterized by clusters of cells invading the lumen of the prostatic ducts and accompanied by a  
72 reduced integrity of the basal epithelial compartment, namely High-Grade Prostatic Intra-epithelial  
73 Neoplasia (HGPIN) [6–8].

74 Among the molecular alterations described in PCa, unquestionably *Ets-related gene (ERG)*  
75 expression is the one with the highest incidence [9–11]. ERG is a member of the ETS-family of  
76 transcription factors, which is expressed in several tissues and involved in many different processes  
77 from cell proliferation and angiogenesis to cell differentiation and apoptosis [12,13].

78 The most common genomic rearrangement of *ERG* gene in prostate cells is a microdeletion in the  
79 q22 region of chromosome 21, which fuses exon 1 of the AR-responsive *Transmembrane Serine*  
80 *Protease 2 (TMPRSS2)* gene with exon 4 of *ERG* gene [14]. Since *TMRPSS2* Ex1 covers the  
81 promoter and 5'UTR region of the gene, the outcome of *TMPRSS2-ERG* fusion is not a chimeric  
82 protein but the *de-novo* AR-driven expression of a delta-40 amino-terminal truncated isoform of ERG  
83 in prostate epithelium [15–17]. *TMPRSS2-ERG* rearrangement is considered a very early event  
84 during prostate tumorigenesis and it is commonly identified in 5-30% of HGPIN prostate lesions [17–  
85 22]. However, several *in vivo* studies exploiting Genetically Engineered Mouse Models (GEMM)  
86 show that the expression of ERG in mouse prostate can, at most, induce benign lesions in the  
87 prostatic epithelium, but never malignant cell transformation and PCa [7,16,23–25]. These findings  
88 are further strengthened by the inability of ERG to trigger cell transformation in immortalized human  
89 prostate cell lines [23–26].

90 Even if the oncogenic role(s) of ERG in PCa have been functionally associated with invasive and  
91 metastatic tumor progression, the presence of genomic rearrangements driving ERG expression in  
92 5-30% of HGPIN prostate lesions is at least counterintuitive and suggests possible critical role(s) of  
93 ERG in the very early stages of prostate tumorigenesis.

94 Here, by combining organoids technology and Click-chemistry approach coupled to Mass  
95 Spectrometry analyses, we demonstrate that ERG expression in prostate progenitors is functional  
96 to compromise normal prostate epithelium homeostasis, and characterize an ERG-dependent  
97 signature of secreted proteins with potential autocrine and paracrine roles in the generation of  
98 permissive conditions for tumor onset.

99

## 100 ***Material and Methods***

### 101 **Mouse Husbandry and Care**

102 Wild-type C57BL/6J (JAX # 000664) mice were purchased from The Jackson Laboratory. Mice were  
103 housed in a certified Animal Facility in accordance with FELASA guidelines and recommendations,  
104 and were in compliance with the Directive 2010/63/UE and its Italian transposition D. L.vo 26/2014.  
105 All animal experiments were performed according to the European Communities Council Directive  
106 (2010/63/EU) and approved by the Italian Ministry of Health and the University of Trento Animal  
107 Welfare Committee (642/2017-PR) as conforming to the relevant regulatory standards.

### 108 **Mouse prostate organoid cultures**

109 Mouse prostate organoids (mPrOs) were generated from prostate glands collected from adult (6-12  
110 months year-old) C57BL/6J wild-type males. Generation and establishment of mPrOs cultures were  
111 achieved as previously described [27–29]. Briefly, single cells or small clumps of cells were  
112 embedded in growth factor reduced Matrigel® (Corning, 356231) or BME-2® (AMSBIO, 3533) and  
113 plated as a 40 µl dome (1,000-2,000 cells/dome) in a 12-well cell culture plate (3 domes/well). Matrix  
114 domes were left to solidify and covered with ENRAD medium including: 50 ng/ml Egf (PeproTech,  
115 315-09), 100 ng/ml Noggin (PeproTech 120-10C), 10% R-Spondin1 (conditioned medium), 200 nM  
116 A83-01 (Tocris, 2393) and 10 nM Dihydrotestosterone (DHT, Merck, 10300). Additionally, the  
117 medium was supplemented with 10 µM Y-27632 (Calbiochem, 146986-50-7; for 24-48 h after  
118 seeding) and with 10 nM ATRA (Merck R2625). Organoids were cultured in a standard tissue culture  
119 incubator. Medium was changed every 2-3 days and mPrOs growth was followed by stereoscopic  
120 analysis (Leica MZ16F). Organoids were passed once a week by recovering cells using 1 mg/ml

121 Dispase II (ThermoFisher Sci.) and TrypLE (ThermoFisher Sci.), and mechanically dissociating into  
122 single cells or small clumps before replating/reseeding.

### 123 **Generation of retroviral vectors and transduction of mPrOs**

124 The retroviral vector pTGMP-ERG<sub>M40</sub> inducible for the expression of ERG was generated as  
125 previously described [26]. To produce retroviral particles, half-confluent HEK-293T cells in antibiotic-  
126 free DMEM medium were transfected with 10 µg of pTGMP-ERG<sub>M40</sub>, 2.5 µg of the envelope pHDM-  
127 VSVG plasmid and 7.5 µg of the packaging pRetro-Gag-Pol plasmid supplemented with 50 µl of  
128 polyethylenimine (PEI, Sigma). Eight hours after transfection the medium was replaced with low FBS  
129 (3-5%) complete medium and, after 48 h, the supernatant was collected, filtrated, quantified [30]  
130 and, finally, stored at -80°C. Stable mPrOs inducible for the expression of ERG were generated as  
131 described below. mPrOs cultures were mechanically dissociated into single cells and counted. The  
132 transduction was performed by spinoculation, mixing 2-3 x 10<sup>5</sup> cells, retroviral particles (0.3  
133 RTU/reaction) and 4 µg/ml polybrene (Sigma, H9268) in a low adhesion 96-well plate. The sample  
134 was centrifuged for 1 h at 600 g. Cells were then gently resuspend, collected into a tube, and further  
135 incubated for 4-6 h at 37°C. After this time, cells were pelleted and seeded as usual. Positive  
136 selection started 48 h after transduction adding 1 µg/mL puromycin (InvivoGen) to the medium and  
137 maintained for 2 weeks. The inducible expression of ERG was stimulated adding 1 µg/ml doxycycline  
138 (Sigma Aldrich) to the medium for at least 96 h. Stable mPrOs were tested and authenticated by  
139 Western blot and RT-qPCR for specific expression of ERG and its activity on known ERG-targeted  
140 genes [24,25].

### 141 **Cell lines**

142 RWPE-1 (#CRL-11609), LNCaP Fast Growing Clone (#CRL-1740) and VCaP (#CRL-2876) cell lines  
143 were purchased from the American Type Culture Collection (ATCC). LNCaP and 22Rv1 prostate  
144 cancer cell lines with inducible expression of ERG were generated in the Demichelis' laboratory with  
145 a vector kindly provided by David Rickman. Cells were cultured in a humidified incubator at 37°C  
146 and 5% CO<sub>2</sub> and maintained according to manufacturer's instructions.

### 147 **Quantitative RT-qPCR and End-point PCR**

148 To collect RNA from mPrOs, 3 domes (1200-1500 cells/dome) were processed for each analyzed  
149 condition. The samples were mechanically dissociated with Dispase II, collected in a tube, incubated  
150 at 37°C for 5 min, washed with 0.1% BSA in PBS and centrifuged (300 g, 5 min) before resuspending  
151 the cell pellet in the provided lysis buffer. RNA was extracted using the RNeasy Plus Micro kit  
152 (Qiagen, 74034) following the manufacturer's protocol. The concentration of the RNA was evaluated  
153 with a NanoDrop™ 2000c spectrophotometer (ThermoFisher Sci) while RNA quality was controlled  
154 via gel electrophoresis. Subsequently, RNA was retrotranscribed into cDNA using iScript™ cDNA  
155 synthesis Kit (Biorad, 1708891) according to the manufacturer's protocol.

156 Quantitative gene expression analysis was achieved through RT-qPCR exploiting the qPCR BIO  
157 SyGreen Mix (PCRBiosystems, PB20.14-05), according to the manufacturer instructions. Reaction  
158 mixes were prepared in final volumes of 10 µl, including 10 ng of cDNAs and gene-specific primers  
159 used at a final concentration of 200 nM. The experiments were performed in three or more technical  
160 replicates using the CFX96 qPCR thermocycler (BioRad) following standard protocols. Results were  
161 processed using the BioRad CFX Manager software (V. 3.1), while gene expression and statistical  
162 analysis were performed through GraphPad PRISM (V. 6.01).

163 End-point PCR amplification was carried out using Phusion Universal qPCR Kit (Life Tech,  
164 F566L), analyzing 50-100 ng of DNA on a C1000 Touch thermal cycler (Biorad). PCR products were  
165 loaded on agarose gels and separated by standard gel electrophoresis. DNA gels were imaged with  
166 an UV scanner (UVITEC). RT-qPCR and End-point PCR analyses were performed with at least 3  
167 independent biological replicates, unless stated in the figure legend; representative data are shown.  
168 Primers are reported in Supplementary Table S1.

### 169 **Subcellular Fractionation and Western blotting**

170 Organoids, usually collected from 6 domes (1200-1500 cells/dome), were washed in ice-cold PBS  
171 twice, pelleted and lysed for 30 min at 4°C with RIPA buffer (50 mM Tris-HCl, pH 7.5, 150 mM NaCl,  
172 1% Triton X-100, 1% sodium deoxycholate, 1% NP-40) supplemented with protease (Halt™ protease  
173 inhibitor cocktail, Life Tech, 87786) and phosphatase inhibitors (Phosphatase-Inhibitor-Mix II  
174 solution, Serva, 3905501). Cell fractionation was performed using NE-PER Nuclear and Cytoplasmic  
175 Extraction Kit (Life Tech, 78833) according to the manufacturer's instructions. Protein concentrations



176 were quantified via BCA assay (Pierce™ BCA protein Assay Kit, ThermoFisher Sci. 23225). Lysates  
177 were resolved by SDS/PAGE and transferred to PVDF membrane (Amersham™ Hybond™, Fisher  
178 Scientific) using a wet electroblotting system (BioRad). The membranes were blocked with 5% non-  
179 fat dry milk or 5% BSA in TBS-T (50 mM Tris-HCl, pH 7.5, 150 mM NaCl, 0.1% Tween20) for 1 h at  
180 RT and then incubated with specific primary antibodies O/N at 4°C (see below). After washes in  
181 TBS-T, membranes were incubated with an HRP-conjugated anti-rabbit (Cell Signaling, 7074) or  
182 HRP-linked anti-mouse (Cell Signaling, 7076) secondary antibody for 1 h at RT. Immunoreactive  
183 bands were detected using ECL LiteAblot plus kit A+B (Euroclone, GEHRPN2235) with an Alliance  
184 LD2 device and software (UVITEC). Western blots were performed in at least 3 independent  
185 biological replicates; representative data are shown. Primary antibodies used were: AR (Santa Cruz,  
186 sc-816), Cytokeratin 5 (Biolegend, 905501), Cytokeratin 8 (Abcam, ab53280), ERG (Abcam,  
187 ab133264), Fibrillarin (Abcam, ab4566), GAPDH (ThermoFisher Sci., MA515738), Nkx3.1 (Millipore,  
188 ab5983), PARP (Cell Signaling, 9542), phosphor-53BP1 (S<sup>25</sup> Abcam, ab70323), phosphor-Atm  
189 (S<sup>1981</sup>, Cell Signaling, 5883), phospho-H2AX (S<sup>139</sup>, Abcam, ab26350), β-Actin (Sigma, A2228), β-  
190 Catenin (Abcam, ab32572), β-Tubulin (Santa Cruz, sc-5274).

### 191 **Egf deprivation experiment**

192 Two days before seeding, mPrOs were treated either with 1 µg/ml doxycycline-containing or mock  
193 medium. Following mechanical dissociation, 1200 cells were seeded in each dome and  
194 supplemented with EGF-deprived medium. After O/N incubation, 1 µg/ml doxycycline was added to  
195 treated samples, changing the medium every 2-3 days. At day 8, organoids were entirely reseeded  
196 in a new dome and doxycycline was added after 24 h, as previously described. Stereoscopic analysis  
197 (Leica MZ16F) was performed daily up to day 14, while viability assay was performed incubating  
198 organoids with 5 µM Calcein-AM (eBioscience, BMS65-0853-78) for 1 h and then analyzing them by  
199 fluorescent stereoscopic imaging.

### 200 **Sample preparation for immunostaining**

201 Organoids were seeded within ECM-like dome, let grow for 48 h and then treated with or without  
202 doxycycline during 72 h. Domes were then enzymatically disaggregated, and organoids were  
203 washed with 0.1% BSA in PBS and embedded in collagen-based matrix (Corning, 354249). After

204 complete polymerization of the domes, complete medium was added to the cultures with the  
205 appropriate treatment and incubated for 24 h. Samples were washed with PBS and fixed with 4%  
206 PFA (Sigma Aldrich, P6148) for 5 h at RT, then collected into histological cassette and subjected to  
207 paraffin embedding. Prostate tissue was harvested, fixed and paraffin embedded using the same  
208 conditions. Formalin-fixed paraffin-embedded (FFPE) blocks were sectioned (5  $\mu\text{m}$ -thick sections),  
209 collected onto glass slides and dried O/N at 37°C.

## 210 **Immunofluorescence**

211 After deparaffinization and antigen retrieval, performed using a citrate-based buffer (pH 6.0) (Vector  
212 Lab, H3300), slides were permeabilized in blocking solution (5% FBS, 0.1% Triton X-100 in PBS)  
213 for 1 h at RT and then incubated O/N at 4°C with primary antibodies. After washing, slides were  
214 incubated with Alexa Fluor conjugated secondary antibodies for 2 h and, before mounting, they were  
215 counterstained with Hoechst 33342 (Abcam, ab145597). All the images were acquired using an Axio  
216 Imager M2 (Zeiss), while image analysis and quantification was performed with ImageJ software  
217 (ImageJ 1.46r NIH). Immunofluorescence studies were performed in at least 3 independent  
218 biological replicates; representative data are shown. The following antibodies were used for  
219 immunofluorescence analysis: Ar (Rabbit, Santa Cruz, sc-816), Cytokeratin 5 (Chicken, Biolegend,  
220 905901), Cytokeratin 8 (Rat, Merck, MABT329), ERG (Rabbit, Abcam, AB92513),  $\beta$ -Catenin (Rabbit,  
221 Abcam, ab32572), Ki67 (Rat, eBioscience, BMS14-5698-82),  $\alpha$ -rabbit Alexa Fluor 488 (Donkey, Life  
222 Technologies, A21208),  $\alpha$ -rat Alexa Fluor 594 (Donkey, Life Technologies, A21209),  $\alpha$ -chicken  
223 Alexa Fluor 633 (Goat, Life Technologies, A21094).

## 224 **Immunohistochemistry**

225 Human prostate samples were retrieved from the archives of the Units of Surgical Pathology of the  
226 S. Chiara Hospital, Trento, Italy (protocol number 1946). Prostate TMA bearing 43 cases of HGPIN  
227 were generated at the Units of Surgical Pathology of the S. Chiara Hospital, while a TMA with 90  
228 cases (60 cases of PCa and adjacent normal tissue + 30 cases of PCa) was purchased from US  
229 Biomax (HProA150PG01). Immunohistochemical analysis was performed at the Department of  
230 Histopathology (S. Chiara Hospital, Trento, Italy) using an automatic immunostainer (BOND-III  
231 platform, Leica Biosystems). Antigen retrieval was carried out with optimized BOND reagents (Bond

232 epitope retrieval solution 1, Leica Biosystems) at pH 6 for 20 min. The following primary antibodies  
233 were used: ERG (Abcam, ab92513/1:500; Biocare, 9FY/1:400), CD68 (NCL-L-CD68, Leica  
234 Biosystems, 1:60), NKX3.1 (Biocare, D2Y1A/1:50), CK-5 (Novocastra, NCL-L-CK5/1:600), P63  
235 (Leica, NCL-p63/1:50). BOND compact polymer detection solution (Leica Biosystems) was used for  
236 the detection. Slides were reviewed independently by two trained pathologists (M.B. and F.G.C).  
237 Images were acquired using an Axio Imager M2 (Zeiss). This study was conducted according to the  
238 guidelines of the Declaration of Helsinki.

### 239 **Flow Cytometry Analysis**

240 Organoids were treated for 4 days with or without 1 µg/ml doxycycline and labeled with 10 µM 5-  
241 ethynyl-2'-deoxyuridine (EdU) for 3 h prior harvesting the samples. mPros were then collected,  
242 washed with 1% BSA in PBS, mechanically dissociated into single cells and filtered through a 30 µm  
243 cup strainer (BD Biosciences). Cells were pelleted and processed with the Click-iT™ Plus EdU Alexa  
244 Fluor™ 488 Flow Cytometry Assay Kit (ThermoFisher Sci, C10632), following the manufacturer's  
245 instructions. DNA content staining was achieved through incubation with TO-PRO™-3 Iodide (Life  
246 Tech, T3695), before proceeding to the analysis. Flow cytometry was performed with a FACS  
247 CantoA flow cytometer (BD Biosciences), and data were analyzed with FlowJo v.10. For FACS  
248 analysis a CantoA flow cytometer (BD Biosciences) was used, and data were analyzed with FlowJo  
249 software (Treestar, V. 10.5.3).

### 250 **Click-iT enrichment of secreted proteins**

251 Organoids were seeded at the desired density, left to grow for 2 days, and then treated with or  
252 without doxycycline for 96 h. Before harvesting the medium, a step of Methionine depletion was  
253 performed culturing cells with Methionine-free medium for 2 h and then labeling samples O/N with  
254 Methionine-free organoid medium containing 0.1 mM L-azidohomoalanine (AHA) labeling agent  
255 (Jena Bioscience). Afterward, medium was recovered, centrifuged and clear supernatant was  
256 transferred in a new tube supplemented with protease and phosphatase inhibitors cocktail. At this  
257 stage, samples were stored at -80°C or immediately processed for secreted, labeled protein  
258 enrichment. Enrichment protocol was based on Click-iT™ protein enrichment kit (ThermoFisher Sci,  
259 C10416) according to the optimized procedures described previously [31,32]. Collected medium was

260 concentrated through centrifugation, mixed with Urea lysis buffer (8 M Urea, 200 mM Tris-HCl, 4%  
261 CHAPS, 1 M NaCl, pH 8) and then incubated with 1 mM Iodoacetamide dissolved in SDS washing  
262 buffer (100 mM Tris-HCl, 1% SDS, 250 mM NaCl, 5 mM EDTA pH 8) for 30 min at 20°C, protected  
263 from light and with mild centrifugation (3,000 - 4,000 g). After that, the sample underwent cyclo-  
264 addition reaction incubating O/N at RT with alkyne matrix and catalyst solution. Reduction-alkylation  
265 steps were performed incubating the sample first with 10 mM DTT for 15 min at 70°C plus additional  
266 15 min at RT, and then with 40 mM Iodoacetamide for 30 min, protected from light. Subsequently,  
267 the resin was resuspended and extensively washed with SDS washing buffer, Tris-Urea washing  
268 buffer (8 M Urea, 100 mM Tris-HCl, pH 8), 20% isopropanol and 20% acetonitrile, respectively. The  
269 resin was then resuspended in digestion buffer (100 mM Tris-HCl, 2 mM CaCl<sub>2</sub>, 10% acetonitrile, pH  
270 8), pelleted and incubated with 2.5 ng/μl MS-grade trypsin (ThermoFisher Sci.) O/N at 37°C with  
271 continuous rotation. After tryptic digestion, samples were centrifuged and the supernatant  
272 transferred in a new tube, while the resin was washed with water, pelleted and the supernatant  
273 added to the same tube to collect as much peptide as possible. Samples were then acidified with  
274 Trifluoroacetic acid and stored at -80°C until MS analysis.

#### 275 **MS analysis**

276 Tryptic peptide mix was first purified by reversed phase (C18) stage tip purification, as previously  
277 described [33] and eluted with a solution of 80% acetonitrile, 0.1% formic acid. The sample was  
278 vacuum dried and then resuspended with a solution of 2% acetonitrile, 0.1% formic acid.

279 LC-MS/MS analysis was performed with an EASY-LC 1000 coupled to a Q-Exactive mass  
280 spectrometer (ThermoFisher Scientific). The analytical nanoLC column is a pulled fused silica  
281 capillary, 75 μm i.d., in-house packed to a length of 12 cm with 3 μm C18 silica particles (Dr. Maisch  
282 GmbH). Peptide mixtures were loaded directly onto the analytical column. A binary gradient was  
283 used for peptide elution. Mobile phase A was composed by 2% acetonitrile/0.1% formic acid,  
284 whereas mobile phase B was 80% acetonitrile/0.1% formic acid. Gradient elution was achieved at  
285 300 nl/min flow rate, ramped from 6% B to 40% B in 90 min, from 40% B to 100% B in 18 min, and  
286 remained at 100% B after additional 10 min. Mobile phase composition was finally brought to 0% B  
287 in 2 min. MS detection was performed on a quadrupole-orbitrap mass spectrometer Q-Exactive

288 (ThermoFisher Scientific) operating in positive ion mode, with nanoelectrospray (nESI) potential at  
289 1800 V applied on the column front-end via a tee piece. Data-dependent acquisition was performed  
290 using a top-12 method with resolution (FWHM), AGC target and maximum injection time (ms) for full  
291 MS and MS/MS of, respectively, 70,000/35,000, 1e6/1e5, 50/120. Mass window for precursor ion  
292 isolation was 1.6 m/z, normalized collision energy was 25, and dynamic exclusion was 25 s. Injected  
293 amounts of samples varied from 4 to 8  $\mu$ l, depending on peptide amount estimated from a preliminary  
294 injection. LC-MS/MS data analysis was conducted using the MaxQuant/Perseus software suite [34].  
295 Label-free quantification was activated in MaxQuant, using default parameters except for the  
296 following: *i*) minimum peak length = 4; *ii*) mass accuracy = 3 ppm; *iii*); retention time window for  
297 match-between-runs options = 0.5 min (match-between-runs was set to "ON", with an alignment time  
298 window of 20 min). Data was searched on the "Mus musculus reference proteome", downloaded on  
299 August 11, 2018 (53,345 sequences). Label free quantification of proteins were based on the LFQ  
300 algorithm [35] and required a minimum of one unique/razor peptide associated to a specific identified  
301 protein.

302 The protein summary output table was loaded in Perseus for statistical and bioinformatic analysis.  
303 After removing hits from reverse and contaminants database and transforming LFQ intensity data in  
304 logarithmic space, proteins were filtered based on valid values (measurement present in at least 2  
305 biological replicates of at least one sample group). Missing values were imputed using default  
306 parameters.

### 307 **Protein network analysis**

308 Analysis of protein-protein interaction network and pathway enrichment were achieved exploiting  
309 STRING V 11.0 web tool (<https://string-db.org/>) [36,37]. Proteins were identified by their unique  
310 Protein ID and were enclosed in the list only if identified in at least 3 different biological replicates  
311 with 2 or more "Unique peptides". Confidence score for the network  $\geq 0.9$ .

### 312 **Heat Map**

313 The heatmap was created using R and RStudio graphic software environment (R Core Team (2019).  
314 R: A language and environment for statistical computing. R Foundation for Statistical Computing,  
315 Vienna, Austria. URL <https://www.R-project.org>; RStudio Team (2018). RStudio: Integrated

316 Development for R. RStudio, Inc., Boston, MA, URL <http://www.rstudio.com>). Data were visualized  
317 using the LFQ intensity value obtained from the MS analysis of each sample. The proteins were  
318 sorted based on the Fold Change value obtained comparing Mock and Doxy mPrOs-ERG and on  
319 the significance of the Fold Change evaluated.

### 320 **TCGA RNAseq Dataset Analysis**

321 Processed RNA-seq counts for TCGA PRAD dataset were downloaded from Recount2 data portal  
322 (PMID:). Counts were scaled and transformed to RPKM values using the recount R package.  
323 Distribution of  $\log_2(\text{RPKM}+1)$  values across normal and tumor samples were compared using two-  
324 sample Wilcoxon test statistics. Correlation between ERG and NKX3-1 transcript levels was  
325 calculated using Pearson correlation and regression line was computed fitting to a linear model.  
326 Provided visual inspection of the distribution of ERG transcript levels across TCGA PRAD tumor  
327 samples, patients presenting an evident over-expression of ERG transcript were selected using a  
328 threshold of  $\log_2(\text{RPKM}+1)$  equal to 3.

### 329 **COMET Assay**

330 Mouse prostate organoids (mPrOs) were seeded at 2,000 cells/dome in a 12-well plate with complete  
331 or Rspo-1 deprived culture medium for 6 days. ERG induction was performed for 96 hours with  
332 doxycycline. After 6 days of culture, mPrOs were dissociated into single cells, harvested by  
333 centrifugation and re-suspended in ice-cold PBS. Cell counts were then normalized to  $1 \times 10^5$   
334 cells/mL. Comet Assay was performed following the manufacturer instructions (Abcam, ab238544).  
335 Briefly, suspended cells were combined with Comet Agarose at 1/10 ratio (v/v) and transferred (75  
336  $\mu\text{L}$ ) on the top of the Comet Agarose Base Layer. The agarose-cell mixture was then dropped onto  
337 slides and let solidify at  $4^\circ\text{C}$  in the dark for 15 minutes before immersion in COMET assay Lysis  
338 Buffer at  $4^\circ$  in the dark for 45 minutes. Excess buffer was then removed and slides were submerged  
339 in freshly prepared Alkaline Electrophoresis Solution at  $4^\circ\text{C}$  in the dark for 30 minutes. When  
340 performed in Alkaline Solution, the COMET assay measures relative levels of DNA single and  
341 double-strand break fragmentation. Gel electrophoresis was then performed at 20 volts (300 mA) for  
342 25 minutes. Slides were then washed twice by immersion in pre-chilled  $\text{dH}_2\text{O}$ . Slides were then fixed  
343 in 70% ethanol for 5 minutes. Following air drying of the agarose, slides were stained with Vista

344 Green DNA Dye and images were collected with a 10x objective lens. COMET tail moments were  
345 then assessed using COMETscore.v2.0 (TriTek Corp., Sumerduck, VA) image processing software  
346 and OpenComet plugin (FIJI – ImageJ) with greater than 100 cells analyzed per condition. Data is  
347 reported as tail moment, which assesses the fluorescence intensity in the tail relative to the head  
348 while accounting for the relative area of both dipoles.

### 349 **Macrophages**

350 Primary mouse Bone Marrow Derived Macrophages (BMDMs) were obtained from femurs of WT  
351 C57B/6J mice (3-6 months of age). Specifically, BM was flushed out with PBS, broke down by  
352 pipetting and gently pelleted. Cells were then resuspended in ACK lysis buffer (Life Tech.,  
353 A1049201), incubated at room temperature for 5 minutes, diluted with PBS and gently pelleted again  
354 to remove lysis buffer. Cells were then resuspended in RPMI culture medium (10% Heat-Inactivated  
355 FBS, 1 mM L-glutamine, 1% Pen/Strep), counted and seeded at about 2 million cells per well of a 6  
356 well plate in culture medium supplemented with 10 ng/ml recombinant M-CSF (SinoBiological,  
357 #51112-MNAH). Macrophages were cultured for 7 days, replacing medium every 2-3 days, in  
358 presence of M-CSF. To induce M1 macrophage polarization, cells are cultured for 48 h with 0.1  
359 ug/ml Lipopolysaccharide (LPS; Sigma, #L4516) and 50 ng/ml recombinant IFN $\gamma$  (SinoBiological,  
360 #50709-MNAH). Interleukin 4 (10 ng/mL; SinoBiological, #51084-MNAE) and interleukin 13 (10  
361 ng/mL; SinoBiological, #50225-MNAH) were used to induce M2 polarization.

362 For the analysis of mPrOs influence, samples were treated with 50% mPrOs conditioned medium,  
363 or unconditioned control, for 48 h while adding the indicated polarization cocktail to the culture  
364 conditions. At the end of the incubation cell were lysed in the provided lysis buffe and RNA was  
365 extracted using the RNeasy Plus Micro kit (Qiagen, 74034) following manufacturer's protocol.

366 RNA was then processed as described in the previous paragraph for RT-qPCR analysis of  
367 selected targets

### 368 **Statistical Analysis**

369 GraphPad Prism 6 software (GraphPad Software Inc.) was used for all statistical analyses applied  
370 to the experimental data. Student t test for unpaired or paired (relative to figure 5) data (two-tailed)  
371 was used to test the probability of significant differences between two groups of samples. Data are

372 presented as mean  $\pm$  SD of at least three independent experiments, unless stated in the figure  
373 legend. Statistical significance is presented as \*  $p \leq 0.05$ , \*\*  $p \leq 0.01$ , \*\*\*  $p \leq 0.001$ . Significant  
374 differences in the amount of secreted proteins across different conditions were assessed for  
375 significance according to the Benjamini-Hochberg method with a FDR  $< 0.2$ . An additional fold-  
376 change cutoff for biological significance was applied (either Fold Changes FC  $> 2$  or FC  $< 0.5$ ).

377

## 378 **Results**

### 379 **ERG influences cell lineage and Egf dependency of mouse prostate progenitors**

380 The recent development of 3D prostate organoids cultures from mouse and human adult prostate  
381 tissue [28,29,38,39] has opened a new window of opportunity for the study of prostate physiology,  
382 tissue homeostasis and tumorigenesis. Taking advantage of this new knowledge, we established a  
383 biobank of mouse prostate organoid (mPrO) lines derived from wild type and genetically engineered  
384 mice of different strains, by pooling the different prostate lobes (ventral, dorsolateral and anterior) or  
385 taking them separately [27].

386 In order to genetically engineer wild type mPrOs with a doxycycline inducible ERG expression  
387 vector system, ERG cDNA was cloned from VCaP cells, a human PCa cell line that carries the  
388 *TMPRSS2-ERG* rearrangement and expresses a shorter form of ERG starting from methionine 40  
389 (ERG<sub>M40</sub>), and inserted through enzymatic restriction into the retroviral pTGMP-rtTA3 plasmid  
390 downstream the TRE-CMV promoter element (pTGMP-ERG<sub>M40</sub>) [26]. Wild type prostate organoids  
391 were generated by pooling together the three prostate lobes of C57BL/6J mice (Figure 1) and  
392 transduced with pTGMP-ERG<sub>M40</sub> bearing viral particles (Supplementary Figure S1A). mPrOs-  
393 ERG<sub>M40</sub> were grown for 4 passages (one month) in presence of puromycin to stabilize the line, then  
394 RT-qPCR and Western blot analyses were run on wild type mPrOs and mPrOs-ERG<sub>M40</sub> treated or  
395 not with 1  $\mu\text{g/ml}$  doxycycline for 96 hours. ERG<sub>M40</sub> was robustly expressed in the mPrOs-ERG<sub>M40</sub>  
396 induced with doxycycline, although a slight amount of ERG<sub>M40</sub> mRNA was also noted in non-induced  
397 mPrOs-ERG<sub>M40</sub> (Figure 2A-B). Nevertheless, immunodetection analyses and gene expression  
398 studies on specific ERG-targeted genes (*Plau*, *Mmp3*, *Fam25c* and *Smim6*) [24,25] showed ERG<sub>M40</sub>



399 protein and the expected transcriptional response exclusively in the mPrOs-ERG<sub>M40</sub> treated with  
400 doxycycline (Figure 2C-D).

401 Immunofluorescence staining for Krt 5 and Krt 8 markers pointed out the diffusion of Krt 8 signal  
402 into the basal cell compartment in doxycycline treated mPrOs-ERG<sub>M40</sub> (Figure 2E and  
403 Supplementary Figure S1B), while immunoblot and RT-qPCR studies showed a significant increase  
404 in the expression of Krt 8 at both mRNA and protein levels in mPrOs-ERG<sub>M40</sub> treated with  
405 doxycycline, which was accompanied by concomitant reduction of Krt 5 levels (Figure 2F-G). We  
406 then analyzed the proliferation rate of wild type mPrOs and mPrOs-ERG<sub>M40</sub> either with or without  
407 doxycycline administration. Quantification of Ki67+ cells in the four different conditions showed a  
408 significant reduction in the number of proliferating cells in ERG<sub>M40</sub> expressing mPrOs (Figure 2H-I).  
409 To carefully investigate the effect of ERG<sub>M40</sub> on cell cycle, wild type and ERG<sub>M40</sub> mPrOs were treated  
410 with 5-ethynyl-2'-deoxyuridine (EdU) and analyzed by flow cytometry. EdU incorporation did not  
411 show any significant alteration in the fraction of cells in active DNA replication in the four different  
412 conditions (Figure 2J). Since Ki67 discriminates proliferating cells regardless of the phase of the cell  
413 cycle in which they are (G1, S, G2 and M) from those in G0, we investigated the consequence of  
414 prolonging ERG<sub>M40</sub> expression in mPrOs. At the end of the first week, doxycycline-treated mPrOs-  
415 ERG<sub>M40</sub> culture showed a barely detectable reduction of organoids size and number. After reseeded,  
416 such differences became much more pronounced at the end of the second week, thus confirming a  
417 mild but consistent effect of ERG<sub>M40</sub> in lowering the proliferative potential of mouse prostate  
418 progenitor cells (Supplementary Figure S2).

419 Besides the deregulation of mechanisms controlling cell proliferation and differentiation, a further  
420 important feature that increases the risk of a neoplastic transformation is the ability of pre-malignant  
421 cells to grow under nutrients and growth factors restrictions.

422 To test this eventuality, wild type and ERG<sub>M40</sub> mPrOs were cultured with or without doxycycline,  
423 and in the presence or absence of Epithelial Growth Factor (EGF) for up to two weeks. Compared  
424 to normal conditions (EGF 50 ng/ml), EGF withdrawal precludes the growth of wild type mPrOs, as  
425 well as of mock ERG<sub>M40</sub> organoids. Contrarily, doxycycline-treated mPrOs-ERG<sub>M40</sub> survive and,

426 albeit slowly, form vital 3D organoids, as observed with calcein labelling (Figure 2K and  
427 Supplementary Figure S2B).

428

#### 429 **ERG expression in mPrOs alters the secreted proteome**

430 Click-chemistry coupled with Mass Spectrometry (Click-MS) is an efficient method for the study of  
431 secreted proteins [31,32].

432 Wild type mPrOs were exposed to AHA for 16 hours, then supernatants were collected and  
433 processed according to the Click-MS protocol (Figure 3A and Supplementary Figure S3; see also  
434 Material and Methods). Four independent biological replicates were analyzed over six months and  
435 more than 200 proteins per replicate were unequivocally identified by at least two unique peptides.  
436 Of note, 172 proteins were recurrently identified in all the 4 biological replicates (Figure 3B and  
437 Supplementary Table S2), thus demonstrating the robustness of the Click-MS approach and the  
438 remarkable stability of wild type mPrOs cultures over time (Cambuli et al., *submitted*; Karthaus et  
439 al., 2014). Importantly, a literature-based study of the identified proteins defined more than 20% of  
440 the hits as already known prostate secreted factors (e.g. Activin A, VEGF, GDF15, MST1, Clusterin,  
441 SBSN, IGFBP3, LCN2, SPON2, LTF, Supplementary Table S2) [40–42], thus further reinforcing the  
442 thesis that mPrOs can be an interesting new biological system to model and study prostate tissue  
443 homeostasis and disease. Proteins that have been identified in at least 3 out of 4 replicates by at  
444 least two unique peptides were included in ontology and protein network studies. Ontology  
445 classification performed with DAVID software V. 6.8 [43,44] showed a significant enrichment of GO  
446 terms associated with the extracellular space, thus demonstrating the robustness of our approach  
447 (Supplementary Table S3). STRING software V 11.0 [37] was used to investigate protein networks.  
448 Data generated from this analysis includes a total number of 216 proteins and shows 3 highly  
449 connected cores of elements: Extracellular matrix (ECM) organization (MMU-1474244), Regulation  
450 of IGF transport and uptake (MMU-381426), and Innate immune system (MMU-168256) (Figure 3C-  
451 D and Supplementary Table S4). Because of the high level of confidence (interaction score  $\geq 0.9$ )  
452 imposed to the analysis, almost 40% of proteins are not connected with any other element meaning  
453 that other interesting networks could potentially emerge by lowering the stringency.

454 Click-it/MS studies were then extended to ERG<sub>M40</sub> mPrOs. Organoids were treated with  
455 doxycycline (1 µg/ml), or left untreated (mock), for 96 hours before AHA labelling. Four independent  
456 biological replicates were analyzed for each condition. Approximately 200 proteins per sample were  
457 identified (by at least two unique peptides), of which 150, 154 and 142 were recurrently found in all  
458 the 4 replicates of wild type mPrOs treated with doxycycline (WT doxy), mPrOs-ERG<sub>M40</sub> left untreated  
459 (ERG mock), and mPrOs-ERG<sub>M40</sub> treated with doxycycline (ERG doxy), respectively (Figure 3E-F,  
460 Supplementary Figure S4A-B and Supplementary Table S5). Then, the number of shared proteins  
461 among the 4 different conditions was analyzed. To increase the coverage of our study, we included  
462 in this analysis proteins identified by minimum 2 unique peptides in at least 3 replicates out of 4. As  
463 shown by the Venn diagram in Figure 3F, the largest fraction of proteins (n=137) was identified in all  
464 the 4 different conditions, while some others resulted exclusively detected in (n=17), or not detected  
465 (n=20), in the supernatant of doxycycline-induced mPrOs-ERG<sub>M40</sub>. MaxQuant label-free  
466 quantification, based on LFQ algorithm and exploiting the MaxQuant/Perseus software suite [34,35]  
467 was used to estimate significant differences in the amount of the secreted proteins between mPrOs  
468 expressing ERG<sub>M40</sub> and those that do not. The heatmap, obtained by plotting the intensity values  
469 calculated for every single identified protein in the 4 replicates of the 4 conditions (Figure 3G),  
470 highlights a signature of secreted proteins whose relative amount in the secretome changes  
471 according to ERG<sub>M40</sub> expression (Supplementary Table S6). Thirty-seven proteins show significant  
472 differences > 2 folds (either Fold Change FC > 2 or FC < 0.5, with significance assessed by the  
473 Benjamini-Hochberg method, FDR < 0.2) in the doxycycline-induced mPrOs-ERGM40 compared to  
474 all other conditions. Among these, Lcn2, C16orf89, Spon2, Spink5 and Ctla2 $\alpha$  are the proteins that  
475 mark the most the mPrOs-ERG<sub>M40</sub> secretome, while Sbsn and Wnt-4 appear substantially  
476 underrepresented (Figure 3H-I). Of note, RT-qPCR analysis demonstrates a significant change in  
477 the expression of these genes in doxycycline treated mPrOs-ERG<sub>M40</sub> (Figure 3J), suggesting  
478 transcriptional control by ERG<sub>M40</sub>.

479

480 **ERG modulates canonical Wnt signaling in prostate progenitors promoting double strand**  
481 **breaks accumulation via Gsk3 $\beta$ -dependent Nkx3.1 degradation**

482 Transcriptional profile data of wild type mPrOs (Cambuli et al., *submitted*) shows robust expression  
483 of all key-components of the canonical Wnt pathway, included several Wnt ligands (Wnt-4, -7a and  
484 -7b, -9a, and -10a) (Supplementary Figure S5A). However, our proteomic studies identify only Wnt-  
485 4 in the supernatant of mPrOs. Of note, Wnt-4 and Rspo1 have been shown to coordinate early  
486 gonads formations in both male and female mouse embryos [45]. Decreased Wnt-4 secretion in  
487 ERG+ organoids accompanied a substantial reduction of nuclear  $\beta$ -Catenin (Figure 4A) and the  
488 transcriptional downregulation of canonical  $\beta$ -Catenin targeted genes, included, unexpectedly, *Lgr4*,  
489 the most expressed Rspo1 receptor in mouse prostate organoids (Figure 4B). A similar molecular  
490 signature was obtained in wild type organoids following Rspo1 deprivation (Supplementary Figure  
491 S5B-C), while combination of ERG induction and Rspo1 depletion almost abrogated  $\beta$ -Catenin  
492 expression in organoids (Figure 4C-E). Of note,  $\beta$ -Catenin preferentially marks the basal (Krt 8  
493 negative) cells of wild type organoids (Figure 4E and Supplementary Figure S5D), and its reduction  
494 in ERG+ mPrOs seems to go hand in hand with expansion of the Krt 8 compartment (Figure 4E and  
495 Supplementary Figure S5D).

496 During prostate development, canonical Wnt-signaling has been demonstrated promoting the  
497 expression of *Nkx3.1*, a pioneering transcription factor essential in the initial commitment and  
498 terminal differentiation of the luminal compartment of the gland epithelium [46,47].

499 The amount of *Nkx3.1* transcript is relatively low in mPrOs (Cambuli et al., *submitted*), and further  
500 declines in the absence of Rspo1 (Figure 5A, left panel). ERG expression substantially increases  
501 the levels of *Nkx3.1* RNA in mPrOs (Figure 5A, middle panel), although the effect is less pronounced  
502 in the absence of Rspo1 (Figure 5A, right panel).

503 Regardless of the amount of transcript, NKX3.1 protein can be tuned via post-transcriptional  
504 mechanisms that regulate protein stability in prostate cells [48–52]. Phosphorylation of Thr-89 and  
505 Thr-96 residues in the N-terminal PEST domain, as well as of Ser-185, Ser-186, Ser-195 and Ser-  
506 196 residues in the carboxy-terminal, of the protein drives ubiquitination and proteasome  
507 degradation of NKX3.1 under normal and stressed conditions (e.g. inflammation), respectively.  
508 However, little is known regarding signaling pathways and kinases involved in the control of NKX3.1  
509 stability [53]. Interestingly, either ERG expression or Rspo1 deprivation alone does not change the

510 amount of Nkx3.1 protein in mPrOs, which is instead severely reduced by the combination of both  
511 (Figure 5B-C and Supplementary Figure S5F). Bortezomib administration restores Nkx3.1 protein  
512 levels in ERG+ mPrOs cultured without Rspo1, thus demonstrating proteasome involvement in  
513 proteolytic degradation of Nkx3.1 (Figure 5D). Of note, Nkx3.1 loss has minor effect on the luminal  
514 drift triggered by ERG in prostate organoids (Supplementary Figure S5G).

515 Decreased levels of NKX3.1 protein are frequently described in PCa and commonly considered  
516 one of the earliest events in prostate tumorigenesis [50,54–56]. Transcriptomic analysis of human  
517 PCa (cBioPortal, <https://www.cbioportal.org>) shows a slight, but significant, increase of *NKX3.1*  
518 expression in tumor compared to normal tissue, which positively correlates with *ERG* expression in  
519 ERG positive PCa (Supplementary Figure S6A-B). Immunohistochemical analyses for ERG and  
520 NKX3.1 expression in human HGPIN and PCa show heterogeneous amounts of NKX3.1 protein in  
521 both ERG positive and ERG negative prostate lesions, with cells characterized by very low levels of  
522 NKX3.1 protein expression (Supplementary Figure S6C and Supplementary Table S7). Notably,  
523 induction of ERG expression in LNCaP and 22Rv1 human PCa cell lines enhances *NKX3.1*  
524 transcription (Supplementary Figure S6D), but substantially lowers the amount of NKX3.1 protein  
525 (Supplementary Figure S6E).

526 ERG promotes DNA double strand breaks in prostate cancer cells (Supplementary Figure S6E)  
527 [57–59], whereas NKX3.1 is involved in DNA damage repair in prostate epithelium [60–64]. Thus,  
528 ERG expression concomitant with loss of NKX3.1 could pose a major threat to genomic stability  
529 since ERG-induced DNA damage in mPrOs accumulates in the absence of Nkx3.1 (Figure 5E-F),  
530 still remaining sub-lethal (Supplementary Figure S7D).

531 Mechanistically, Rspo1 withdrawal in ERG+ mPrOs leads to massive  $\beta$ -Catenin degradation likely  
532 dependent by a profuse activity of Gsk3 $\beta$ , as suggested by the administration of the Gsk3 $\beta$  inhibitor  
533 CHIR99021 (Supplementary Figure S7A-D). *In silico* prediction studies define Ser-185 and Ser-195  
534 residues of both human and mouse NKX3.1 proteins as putative targets of Gsk3 $\beta$ . Similar to  $\beta$ -  
535 Catenin, CHIR99021 administration completely rescues Nkx3.1 protein levels and, in turn, reduces  
536 the amount of DNA damages in ERG+ mPrOs cultured without Rspo1 (Figure 5F).

537

**538 ERG-dependent paracrine signals influence *Arginase 1* expression in M1 macrophages**

539 Tumorigenesis is considered an unfavorable event. Nutrient unbalance, changes in the activity of  
540 specific cellular pathways, uncontrolled proliferation and dedifferentiation are all crucial stress factors  
541 that trigger immediate cell autonomous and non-cell autonomous responses. Besides activation of  
542 potent tumor suppressive cellular pathways, innate and adaptive immune systems are rapidly  
543 recruited in areas of tissue abnormalities with the primary intent to eradicate atypical cells.  
544 Macrophages are an essential component of the innate immune system, a major constituent of  
545 normal tissues, and key players in tissue repair and remodeling under both homeostatic and stress  
546 conditions. However, epidemiological and clinical studies have defined macrophage-promoted  
547 chronic inflammation as a critical risk factor in epithelial tissues tumorigenesis [65]. Analysis of the  
548 wild type mPrOs secretome pointed out a robust connection between extracellular signals secreted  
549 by prostate progenitors and the innate immune system. Several deregulated proteins in mPrOs-  
550 ERG<sub>M40</sub> supernatants are known to have specific roles in macrophage functions (Figure 6A), and  
551 CD68+ macrophages were found to infiltrate ERG+ HGPIN lesions in human prostates (Figure 6B;  
552 Supplementary Figure S8A). To investigate possible roles of ERG in promoting a pro-inflammatory  
553 tissue microenvironment, primary macrophages derived from femurs of wild type mice were treated  
554 with IFN $\gamma$  and LPS to induce the M1 polarization (Supplementary Figure S8B) and exposed to the  
555 supernatant of wild type and ERG<sub>M40</sub> mPrOs either treated or not with doxycycline (Figure 6C). Forty-  
556 eight hours later, expression of the M1 markers *Il1b*, *Tnf $\alpha$*  and *iNos*, and M2 markers *Arg1* and *Chil3*  
557 was analyzed by RT-qPCR (Figure 6D). Compared to the unconditioned medium, all supernatants  
558 decrease the expression of *Il1b* and *Tnf $\alpha$*  in M1 macrophages, leave *iNos* induction unaffected, but  
559 promote *Arginase 1*, not *Chil3*, transcription (Figure 6D), which lowers the production of nitric oxide  
560 (NO) in M1 macrophages by competing with *iNos* for arginine metabolism. Interestingly, *Arginase 1*  
561 induction is significantly weaker in M1 macrophages conditioned with the supernatants of ERG+  
562 mPrOs than in all other conditions (Figure 6E), supporting the thesis of a possible non-cell-  
563 autonomous function of ERG dedicated to transform inflammatory macrophages in a source of sub-  
564 lethal oxidative stress.

565

566 **Discussion**

567 Being the most prevalent alteration in prostate cancer, ERG rearrangement was heavily studied in  
568 the past years from many different groups. *ERG* genomic rearrangement and expression is  
569 considered a very early event in the history of PCa, being identified in a significant fraction of HGPIN  
570 prostate lesions [18–22]. However, *in vitro* and *in vivo* experiments show that ERG expression *per*  
571 *se* is not sufficient to induce full prostate cell transformation [7,16,23–25], while it has been robustly  
572 associated to increased migratory and invasive potential of immortalized and malignant prostate  
573 cells [9,17,23,26]. Therefore, expression of ERG in early prostate lesions is hardly justified by its  
574 involvement in PCa progression towards more advanced stages of the disease.

575 In *Pten/Trp53* double-null mouse model of PCa, ERG expression lowers tumor aggressiveness  
576 by decreasing proliferation and promoting luminal differentiation of cancer cells [66]. ERG expression  
577 in mouse prostate organoids promotes prostate progenitors commitment towards the luminal lineage  
578 (Figure 7 and [67]. Importantly, expansion of the luminal compartment occurs with concomitant  
579 contraction of the basal layer in prostate organoids (Figure 7), which resembles the histologic feature  
580 of the HGPIN lesions [7].

581 Thinking about the possible barriers that pre-malignant cells have to overcome to potentially  
582 develop a frank prostatic carcinoma, proliferation in the absence of stimuli is a top priority [68]. A  
583 further important feature of ERG<sub>M40</sub> expressing mPrOs is their ability to grow in absence of EGF, a  
584 condition that is not permissive for the growth of mouse prostate organoids (Cambuli et al.,  
585 *submitted*; Chua et al., 2014; Drost et al., 2016; Karthaus et al., 2014). This result suggests that  
586 ERG<sub>M40</sub> expression in normal prostate cells could uncouple them from the proliferative signals  
587 controlling tissue homeostasis, thus making ERG+ HGPIN cells “*master of their own destiny*” [68].  
588 Among the proteins differentially secreted by ERG<sub>M40</sub> expressing mPrOs, Macrophage stimulating  
589 1/Hepatocyte growth factor-like (Mst1), Angiogenin (Ang), Growth differentiation factor 15/Prostate  
590 derived factor/Macrophage inhibitory cytokine 1 (Gdf15), and Vegf $\alpha$  are of particular interest in this  
591 scenario because they are over-expressed/secreted in human prostate cancer and responsible for  
592 activating pro-survival and pro-proliferation pathways in prostate cancer cells [69–73]. Future studies

593 will help disentangling the possible contribution of those factors to sustain ERG+ pre-malignant  
594 prostate cells under limited growth conditions.

595 On the other hand, the lower number of Ki67+ cells, which marks all phases of the cell cycle with  
596 the exclusion of G<sub>0</sub>, in presence of unaffected cell cycle might suggest a role of ERG in the transition  
597 of proliferating prostate cells to a more quiescent status. Although in 3D prostate organoids, as well  
598 as in HGPIN prostate lesions, ERG activity is not sufficient *per se* to induce cell motility, according  
599 to the “go-or-grow” hypothesis this finding potentially highlights new traits of the pro-migratory  
600 phenotype that ERG expression establishes in malignant prostate cells.

601 Besides ERG expression, loss of NKX3.1 is also a very common condition in human PCa, and  
602 one of the few molecular alterations functionally associated with the early stages of tumorigenesis  
603 [48,74–77]. During mouse prostate organogenesis, Wnt signaling released from the urogenital  
604 stroma stimulates *Nkx3.1* expression in all the epithelial cells of ductal buds [46]. Here, *Nkx3.1*  
605 preserves luminal stem cells, promotes differentiation of the luminal compartment by controlling the  
606 rate at which proliferating luminal cells exit the cell cycle, and regulates ductal morphogenesis  
607 [47,78–80]. In addition to its crucial role in controlling the homeostasis of the luminal compartment  
608 of the prostate, NKX3.1 safeguards genome stability in prostate cells by promoting DNA damage  
609 repair [60,61][81] and protect mitochondria from the harmful effects of oxidative stress [63].  
610 Heterozygous loss of *Nkx3.1* in adult mouse prostate generates hyperplastic and dysplastic pre-  
611 malignant epithelial lesions resembling human HGPIN [77,78,82]. Of note, F4/80+ macrophages are  
612 among the most abundant immune cells infiltrating the *Nkx3.1*-null mouse prostates, where they play  
613 a pivotal role in the development of HGPIN lesions by establishing a chronically inflamed oxidative  
614 microenvironment [83]. NKX3.1 expression is significantly reduced in almost 50% of HGPIN lesions  
615 [48,55,75]. Remarkably, NKX3.1 represses *ERG* transcription in prostate cells [84] and disfavors  
616 TMPRSS2-ERG genomic rearrangement [85], which supports the hypothesis that 8p21 deletions  
617 (NKX3.1) may precede 21q22 rearrangements (TMPRSS2-ERG fusion) in human prostate cancer  
618 harboring both molecular alterations [86]. However, ERG silences *NKX3.1* expression epigenetically  
619 [87] and promotes NKX3.1 protein degradation (Figure 7), which implicates the possible reverse  
620 sequence of these two early events in prostate tumorigenesis. An important consequence of the



621 coexistence of ERG expression and NKX3.1 loss in prostate cells is the substantial increase in DNA  
622 damage (Figure 7). Recently, Hong and colleagues described a prominent role of ATR/CHK1  
623 kinases - commonly activated by replication fork stalling - in promoting ERG proteolysis, while, in  
624 contrast, ATM/CHK2 signaling, triggered by DNA double strand breaks (DSBs), does play no roles  
625 [88]. Likely, by favoring DSBs formation in prostate cells, ERG imposes a selective pressure on DSB  
626 repair pathways that might explain the frequent loss of DSBs repair effectors (e.g. P53, BRCA2,  
627 ATM) in ERG+ human PCa [75].

628 Aberrant proliferation and genomic instability are pre-requisite for tumorigenesis, but it may be  
629 not sufficient in a complex environment such as a tissue. It is well-known that inflammation and  
630 immune activated cells play pivotal roles in the very early stage of the tumorigenic transformation  
631 [65]. Pre-cancerous cells need to influence and hijack immune response to “*avoid immune*  
632 *destruction*” [68]. Noteworthy, several proteins differentially secreted by ERG<sub>M40</sub> prostate organoids  
633 have been shown to influence the immune system, primarily macrophages. Pro-inflammatory  
634 macrophages release cytotoxic molecules and reactive oxygen species like nitrogen intermediates  
635 to trigger cell death. We have found that prostate organoids lessen the killing weaponry of M1  
636 macrophages through secreted signals. This ability might be crucial *in vivo* to protect adult progenitor  
637 cells, and their regenerative potential, from the frequent inflammatory conditions affecting prostate  
638 gland, especially in aged men. Supernatants of ERG<sub>M40</sub> mPrOs still reduce the expression of  
639 cytotoxic molecules (e.g., Tnf $\alpha$  and Il1 $\beta$ ) in M1 macrophages, but *Arginase 1* expression is  
640 significantly less induced. This condition should favor the production of nitric oxide (NO) from the  
641 catabolism of arginine through iNOS/Nos2 activity. Thus, by establishing a focal source of sub-lethal  
642 oxidative stress in the microenvironment, ERG could increase the rate of genetic and genomic  
643 alterations in prostate epithelial cells (Figure 7).

644 To conclude, we speculate that by creating a sophisticated network of autocrine and paracrine  
645 extracellular signals in pre-cancerous human prostate lesions, ERG may orchestrate the prelude to  
646 malignant transformation.

647

648

649 **Acknowledgments**

650 We are grateful to Alberto Inga and Fulvio Chiacchiera for fruitful discussions. We thank current and  
651 former members of the Lunardi laboratory for experimental support and advice. We are grateful to  
652 Dr Luca Morelli and all the staff at the Department of Histopathology (S. Chiara Hospital, Trento,  
653 Italy) for their technical support with the histological work. Furthermore, we thank all the staff at the  
654 CIBIO core facilities for their help. Illustrations were created with Inkscape and BioRender.com. This  
655 work was funded by the Giovanni Armenise-Harvard Foundation (Career Development Award to  
656 A.L.; by the Lega Italiana Lotta ai Tumori (LILT-Bolzano) to A.L.; by the Italian Ministry of University  
657 and Research (PRIN 20174PLLYN) to A.L.; by core funding from the Department of Cellular,  
658 Computational, and Integrative Biology-CIBIO to A.L.; by the Italian Ministry of University and  
659 Research (PRIN 20174PLLYN) to V.P.; by Associazione Italiana per la Ricerca sul Cancro (AIRC-  
660 IG 24851) to V.P.; by the Italian Ministry University and Research (PRIN-2017HWTP2K\_004 and  
661 MIUR-ARS01\_00876) to G.D.S.; by the Associazione Italiana per la Ricerca sul Cancro (AIRC  
662 Special Program 5x1000, 22759) to G.D.S; by the Associazione Italiana per la Ricerca sul Cancro  
663 (AIRC-IG 22174) to G.D.S; by the INTERREG V-A Italia-Austria P-CARE (ITAT1050) to G.D.S; by  
664 the Ministero della Salute (RF-2019-12368718) to G.D.S.; by the European Research Council (ERC)  
665 under the European Union's Horizon 2020 research and innovation program (grant agreement No  
666 648670) to F.D; by the Prostate Cancer Foundation (19YOUN16) to F.L; by the Associazione Italiana  
667 per la Ricerca sul Cancro (AIRC MFAG 2017-ID 20621) to A.R.; by the Italian Ministry of University  
668 and Research (PRIN 20174PLLYN) to M.G.; by the University of Trento (Starting Grants Young  
669 Researchers 2019) to A.A. Individual fellowships were awarded from the European Union (H2020-  
670 MSCA 749795 to A.Be.), the Fondazione Umberto Veronesi (FUV 2016 to A.A. and F.C., FUV 2017  
671 to F.C., and FUV 2018 to A.B.), the European Molecular Biology Organization (EMBO Short  
672 Fellowship to M.L.) and the University of Trento (Ph.D. fellowship to D.D.F, and V.F.).

673

674

675

676

677 **References**

- 678 [1] J. Ferlay, I. Soerjomataram, R. Dikshit, S. Eser, C. Mathers, M. Rebelo, D.M. Parkin, D.  
679 Forman, F. Bray, Cancer incidence and mortality worldwide: sources, methods and major  
680 patterns in GLOBOCAN 2012, *Int J Cancer*. 136 (2015) E359-386.  
681 <https://doi.org/10.1002/ijc.29210>.
- 682 [2] G. Attard, C. Parker, R.A. Eeles, F. Schröder, S.A. Tomlins, I. Tannock, C.G. Drake, J.S. de  
683 Bono, Prostate cancer, *Lancet*. 387 (2016) 70–82. [https://doi.org/10.1016/S0140-6736\(14\)61947-4](https://doi.org/10.1016/S0140-6736(14)61947-4).
- 685 [3] R. Hodson, Prostate cancer: 4 big questions, *Nature*. 528 (2015) S137.  
686 <https://doi.org/10.1038/528S137a>.
- 687 [4] T. Nyberg, D. Frost, D. Barrowdale, D.G. Evans, E. Bancroft, J. Adlard, M. Ahmed, J. Barwell,  
688 A.F. Brady, C. Brewer, J. Cook, R. Davidson, A. Donaldson, J. Eason, H. Gregory, A.  
689 Henderson, L. Izatt, M.J. Kennedy, C. Miller, P.J. Morrison, A. Murray, K.-R. Ong, M. Porteous,  
690 C. Pottinger, M.T. Rogers, L. Side, K. Snape, L. Walker, M. Tischkowitz, R. Eeles, D.F. Easton,  
691 A.C. Antoniou, Prostate Cancer Risks for Male BRCA1 and BRCA2 Mutation Carriers: A  
692 Prospective Cohort Study, *Eur Urol*. 77 (2020) 24–35.  
693 <https://doi.org/10.1016/j.eururo.2019.08.025>.
- 694 [5] M.M. Shen, C. Abate-Shen, Molecular genetics of prostate cancer: new prospects for old  
695 challenges, *Genes Dev*. 24 (2010) 1967–2000. <https://doi.org/10.1101/gad.1965810>.
- 696 [6] D.G. Bostwick, J. Qian, High-grade prostatic intraepithelial neoplasia, *Mod Pathol*. 17 (2004)  
697 360–379. <https://doi.org/10.1038/modpathol.3800053>.
- 698 [7] O. Klezovitch, M. Risk, I. Coleman, J.M. Lucas, M. Null, L.D. True, P.S. Nelson, V. Vasioukhin,  
699 A causal role for ERG in neoplastic transformation of prostate epithelium, *Proc Natl Acad Sci U S A*. 105 (2008) 2105–2110. <https://doi.org/10.1073/pnas.0711711105>.
- 701 [8] R. Montironi, R. Mazzucchelli, A. Lopez-Beltran, L. Cheng, M. Scarpelli, Mechanisms of  
702 disease: high-grade prostatic intraepithelial neoplasia and other proposed preneoplastic  
703 lesions in the prostate, *Nat Clin Pract Urol*. 4 (2007) 321–332.  
704 <https://doi.org/10.1038/ncpuro0815>.
- 705 [9] F. Demichelis, M.A. Rubin, TMPRSS2-ETS fusion prostate cancer: biological and clinical  
706 implications, *J Clin Pathol*. 60 (2007) 1185–1186. <https://doi.org/10.1136/jcp.2007.046557>.
- 707 [10] C. Kumar-Sinha, S.A. Tomlins, A.M. Chinnaiyan, Recurrent gene fusions in prostate cancer,  
708 *Nat Rev Cancer*. 8 (2008) 497–511. <https://doi.org/10.1038/nrc2402>.
- 709 [11] J. Yu, J. Yu, R.-S. Mani, Q. Cao, C.J. Brenner, X. Cao, X. Wang, L. Wu, J. Li, M. Hu, Y. Gong,  
710 H. Cheng, B. Laxman, A. Vellaichamy, S. Shankar, Y. Li, S.M. Dhanasekaran, R. Morey, T.  
711 Barrette, R.J. Lonigro, S.A. Tomlins, S. Varambally, Z.S. Qin, A.M. Chinnaiyan, An integrated  
712 network of androgen receptor, polycomb, and TMPRSS2-ERG gene fusions in prostate cancer  
713 progression, *Cancer Cell*. 17 (2010) 443–454. <https://doi.org/10.1016/j.ccr.2010.03.018>.
- 714 [12] S.A. Lacadie, L.I. Zon, The ERGonomics of hematopoietic stem cell self-renewal, *Genes Dev*.  
715 25 (2011) 289–293. <https://doi.org/10.1101/gad.2031511>.
- 716 [13] S.J. Loughran, E.A. Kruse, D.F. Hacking, C.A. de Graaf, C.D. Hyland, T.A. Willson, K.J. Henley,  
717 S. Ellis, A.K. Voss, D. Metcalf, D.J. Hilton, W.S. Alexander, B.T. Kile, The transcription factor  
718 Erg is essential for definitive hematopoiesis and the function of adult hematopoietic stem cells,  
719 *Nat Immunol*. 9 (2008) 810–819. <https://doi.org/10.1038/ni.1617>.
- 720 [14] S.A. Tomlins, D.R. Rhodes, S. Perner, S.M. Dhanasekaran, R. Mehra, X.-W. Sun, S.  
721 Varambally, X. Cao, J. Tchinda, R. Kuefer, C. Lee, J.E. Montie, R.B. Shah, K.J. Pienta, M.A.  
722 Rubin, A.M. Chinnaiyan, Recurrent fusion of TMPRSS2 and ETS transcription factor genes in  
723 prostate cancer, *Science*. 310 (2005) 644–648. <https://doi.org/10.1126/science.1117679>.
- 724 [15] F. Demichelis, K. Fall, S. Perner, O. Andrén, F. Schmidt, S.R. Setlur, Y. Hoshida, J.-M.  
725 Mosquera, Y. Pawitan, C. Lee, H.-O. Adami, L.A. Mucci, P.W. Kantoff, S.-O. Andersson, A.M.  
726 Chinnaiyan, J.-E. Johansson, M.A. Rubin, TMPRSS2:ERG gene fusion associated with lethal  
727 prostate cancer in a watchful waiting cohort, *Oncogene*. 26 (2007) 4596–4599.  
728 <https://doi.org/10.1038/sj.onc.1210237>.
- 729 [16] J.C. King, J. Xu, J. Wongvipat, H. Hieronymus, B.S. Carver, D.H. Leung, B.S. Taylor, C.  
730 Sander, R.D. Cardiff, S.S. Couto, W.L. Gerald, C.L. Sawyers, Cooperativity of TMPRSS2-ERG

- 731 with PI3-kinase pathway activation in prostate oncogenesis, *Nat Genet.* 41 (2009) 524–526.  
 732 <https://doi.org/10.1038/ng.371>.
- 733 [17] S. Perner, F.H. Schmidt, M.D. Hofer, R. Kuefer, M. Rubin, [TMPRSS2-ETS gene fusion in  
 734 prostate cancer], *Urologe A.* 46 (2007) 754–760. <https://doi.org/10.1007/s00120-007-1347-0>.
- 735 [18] H. He, A.O. Osunkoya, P. Carver, S. Falzarano, E. Klein, C. Magi-Galluzzi, M. Zhou,  
 736 Expression of ERG protein, a prostate cancer specific marker, in high grade prostatic  
 737 intraepithelial neoplasia (HGPIN): lack of utility to stratify cancer risks associated with HGPIN,  
 738 *BJU Int.* 110 (2012) E751-755. <https://doi.org/10.1111/j.1464-410X.2012.11557.x>.
- 739 [19] S.L. Lee, D. Yu, C. Wang, R. Saba, S. Liu, K. Trpkov, B. Donnelly, T.A. Bismar, ERG  
 740 Expression in Prostate Needle Biopsy: Potential Diagnostic and Prognostic Implications, *Appl*  
 741 *Immunohistochem Mol Morphol.* 23 (2015) 499–505.  
 742 <https://doi.org/10.1097/PAI.000000000000119>.
- 743 [20] C.L. Morais, L.B. Guedes, J. Hicks, A.S. Baras, A.M. De Marzo, T.L. Lotan, ERG and PTEN  
 744 status of isolated high-grade PIN occurring in cystoprostatectomy specimens without invasive  
 745 prostatic adenocarcinoma, *Hum Pathol.* 55 (2016) 117–125.  
 746 <https://doi.org/10.1016/j.humpath.2016.04.017>.
- 747 [21] J.-M. Mosquera, S. Perner, E.M. Genega, M. Sanda, M.D. Hofer, K.D. Mertz, P.L. Paris, J.  
 748 Simko, T.A. Bismar, G. Ayala, R.B. Shah, M. Loda, M.A. Rubin, Characterization of TMPRSS2-  
 749 ERG fusion high-grade prostatic intraepithelial neoplasia and potential clinical implications, *Clin*  
 750 *Cancer Res.* 14 (2008) 3380–3385. <https://doi.org/10.1158/1078-0432.CCR-07-5194>.
- 751 [22] L.H. Teng, C. Wang, M. Dolph, B. Donnelly, T.A. Bismar, ERG Protein Expression Is of Limited  
 752 Prognostic Value in Men with Localized Prostate Cancer, *ISRN Urol.* 2013 (2013) 786545.  
 753 <https://doi.org/10.1155/2013/786545>.
- 754 [23] B.S. Carver, J. Tran, A. Gopalan, Z. Chen, S. Shaikh, A. Carracedo, A. Alimonti, C. Nardella,  
 755 S. Varmeh, P.T. Scardino, C. Cordon-Cardo, W. Gerald, P.P. Pandolfi, Aberrant ERG  
 756 expression cooperates with loss of PTEN to promote cancer progression in the prostate, *Nat*  
 757 *Genet.* 41 (2009) 619–624. <https://doi.org/10.1038/ng.370>.
- 758 [24] Y. Chen, P. Chi, S. Rockowitz, P.J. Iaquina, T. Shamu, S. Shukla, D. Gao, I. Sirota, B.S.  
 759 Carver, J. Wongvipat, H.I. Scher, D. Zheng, C.L. Sawyers, ETS factors reprogram the androgen  
 760 receptor cistrome and prime prostate tumorigenesis in response to PTEN loss, *Nat Med.* 19  
 761 (2013) 1023–1029. <https://doi.org/10.1038/nm.3216>.
- 762 [25] S.A. Tomlins, B. Laxman, S. Varambally, X. Cao, J. Yu, B.E. Helgeson, Q. Cao, J.R. Prensner,  
 763 M.A. Rubin, R.B. Shah, R. Mehra, A.M. Chinnaiyan, Role of the TMPRSS2-ERG gene fusion  
 764 in prostate cancer, *Neoplasia.* 10 (2008) 177–188. <https://doi.org/10.1593/neo.07822>.
- 765 [26] A. Alaimo, M. Lorenzoni, P. Ambrosino, A. Bertossi, A. Bisio, A. Macchia, E. Zoni, S. Genovesi,  
 766 F. Cambuli, V. Foletto, D. De Felice, M.V. Soldovieri, I. Mosca, F. Gandolfi, M. Brunelli, G.  
 767 Petris, A. Cereseto, A. Villarroel, G. Thalmann, F.G. Carbone, M. Kruihof-de Julio, M.  
 768 Barbareschi, A. Romanel, M. Tagliatalata, A. Lunardi, Calcium cytotoxicity sensitizes prostate  
 769 cancer cells to standard-of-care treatments for locally advanced tumors, *Cell Death Dis.* 11  
 770 (2020) 1039. <https://doi.org/10.1038/s41419-020-03256-5>.
- 771 [27] F. Cambuli, V. Foletto, A. Alaimo, D. De Felice, F. Gandolfi, M.D. Palumbieri, M. Zaffagni, S.  
 772 Genovesi, M. Lorenzoni, M. Celotti, E. Bertossio, G. Mazzerio, A. Bertossi, A. Bisio, F.  
 773 Berardinelli, A. Antoccia, M. Gaspari, M. Barbareschi, M. Fiorentino, M.M. Shen, M. Loda, A.  
 774 Romanel, A. Lunardi, Intra-epithelial non-canonical Activin A signalling safeguards prostate  
 775 progenitor quiescence, *Cancer Biology*, 2021. <https://doi.org/10.1101/2021.03.05.433921>.
- 776 [28] J. Drost, W.R. Karthaus, D. Gao, E. Driehuis, C.L. Sawyers, Y. Chen, H. Clevers, Organoid  
 777 culture systems for prostate epithelial and cancer tissue, *Nat Protoc.* 11 (2016) 347–358.  
 778 <https://doi.org/10.1038/nprot.2016.006>.
- 779 [29] W.R. Karthaus, P.J. Iaquina, J. Drost, A. Gracanin, R. van Boxtel, J. Wongvipat, C.M. Dowling,  
 780 D. Gao, H. Begthel, N. Sachs, R.G.J. Vries, E. Cuppen, Y. Chen, C.L. Sawyers, H.C. Clevers,  
 781 Identification of multipotent luminal progenitor cells in human prostate organoid cultures, *Cell.*  
 782 159 (2014) 163–175. <https://doi.org/10.1016/j.cell.2014.08.017>.
- 783 [30] M. Pizzato, O. Erlwein, D. Bonsall, S. Kaye, D. Muir, M.O. McClure, A one-step SYBR Green  
 784 I-based product-enhanced reverse transcriptase assay for the quantitation of retroviruses in  
 785 cell culture supernatants, *J Virol Methods.* 156 (2009) 1–7.  
 786 <https://doi.org/10.1016/j.jviromet.2008.10.012>.

- 787 [31] K. Eichelbaum, J. Krijgsveld, Combining pulsed SILAC labeling and click-chemistry for  
788 quantitative secretome analysis, *Methods Mol Biol.* 1174 (2014) 101–114.  
789 [https://doi.org/10.1007/978-1-4939-0944-5\\_7](https://doi.org/10.1007/978-1-4939-0944-5_7).
- 790 [32] K. Eichelbaum, M. Winter, M. Berriel Diaz, S. Herzig, J. Krijgsveld, Selective enrichment of  
791 newly synthesized proteins for quantitative secretome analysis, *Nat Biotechnol.* 30 (2012) 984–  
792 990. <https://doi.org/10.1038/nbt.2356>.
- 793 [33] J. Rappsilber, M. Mann, Y. Ishihama, Protocol for micro-purification, enrichment, pre-  
794 fractionation and storage of peptides for proteomics using StageTips, *Nat Protoc.* 2 (2007)  
795 1896–1906. <https://doi.org/10.1038/nprot.2007.261>.
- 796 [34] S. Tyanova, T. Temu, P. Sinitcyn, A. Carlson, M.Y. Hein, T. Geiger, M. Mann, J. Cox, The  
797 Perseus computational platform for comprehensive analysis of (prote)omics data, *Nat Methods.*  
798 13 (2016) 731–740. <https://doi.org/10.1038/nmeth.3901>.
- 799 [35] J. Cox, M.Y. Hein, C.A. Luber, I. Paron, N. Nagaraj, M. Mann, Accurate proteome-wide label-  
800 free quantification by delayed normalization and maximal peptide ratio extraction, termed  
801 MaxLFQ, *Mol Cell Proteomics.* 13 (2014) 2513–2526.  
802 <https://doi.org/10.1074/mcp.M113.031591>.
- 803 [36] C. von Mering, M. Huynen, D. Jaeggi, S. Schmidt, P. Bork, B. Snel, STRING: a database of  
804 predicted functional associations between proteins, *Nucleic Acids Res.* 31 (2003) 258–261.  
805 <https://doi.org/10.1093/nar/gkg034>.
- 806 [37] D. Szklarczyk, A.L. Gable, D. Lyon, A. Junge, S. Wyder, J. Huerta-Cepas, M. Simonovic, N.T.  
807 Doncheva, J.H. Morris, P. Bork, L.J. Jensen, C. von Mering, STRING v11: protein-protein  
808 association networks with increased coverage, supporting functional discovery in genome-wide  
809 experimental datasets, *Nucleic Acids Res.* 47 (2019) D607–D613.  
810 <https://doi.org/10.1093/nar/gky1131>.
- 811 [38] C.W. Chua, M. Shibata, M. Lei, R. Toivanen, L.J. Barlow, S.K. Bergren, K.K. Badani, J.M.  
812 McKiernan, M.C. Benson, H. Hibshoosh, M.M. Shen, Single luminal epithelial progenitors can  
813 generate prostate organoids in culture, *Nat Cell Biol.* 16 (2014) 951–961, 1–4.  
814 <https://doi.org/10.1038/ncb3047>.
- 815 [39] D. Gao, I. Vela, A. Sboner, P.J. Iaquinta, W.R. Karthaus, A. Gopalan, C. Dowling, J.N. Wanjala,  
816 E.A. Undvall, V.K. Arora, J. Wongvipat, M. Kossai, S. Ramazanoglu, L.P. Barboza, W. Di, Z.  
817 Cao, Q.F. Zhang, I. Sirota, L. Ran, T.Y. MacDonald, H. Beltran, J.-M. Mosquera, K.A. Touijer,  
818 P.T. Scardino, V.P. Laudone, K.R. Curtis, D.E. Rathkopf, M.J. Morris, D.C. Danila, S.F. Slovin,  
819 S.B. Solomon, J.A. Eastham, P. Chi, B. Carver, M.A. Rubin, H.I. Scher, H. Clevers, C.L.  
820 Sawyers, Y. Chen, Organoid cultures derived from patients with advanced prostate cancer,  
821 *Cell.* 159 (2014) 176–187. <https://doi.org/10.1016/j.cell.2014.08.016>.
- 822 [40] A. Nurdin, Y. Hoshi, T. Yoneyama, E. Miyauchi, M. Tachikawa, M. Watanabe, T. Terasaki,  
823 Global and Targeted Proteomics of Prostate Cancer Cell Secretome: Combination of 2-  
824 Dimensional Image-Converted Analysis of Liquid Chromatography and Mass Spectrometry and  
825 In Silico Selection Selected Reaction Monitoring Analysis, *J Pharm Sci.* 105 (2016) 3440–3452.  
826 <https://doi.org/10.1016/j.xphs.2016.08.013>.
- 827 [41] M.P. Pavlou, E.P. Diamandis, The cancer cell secretome: a good source for discovering  
828 biomarkers?, *J Proteomics.* 73 (2010) 1896–1906. <https://doi.org/10.1016/j.jprot.2010.04.003>.
- 829 [42] S. Principe, Y. Kim, S. Fontana, V. Ignatchenko, J.O. Nyalwidhe, R.S. Lance, D.A. Troyer, R.  
830 Alessandro, O.J. Semmes, T. Kislinger, R.R. Drake, J.A. Medin, Identification of prostate-  
831 enriched proteins by in-depth proteomic analyses of expressed prostatic secretions in urine, *J*  
832 *Proteome Res.* 11 (2012) 2386–2396. <https://doi.org/10.1021/pr2011236>.
- 833 [43] D.W. Huang, B.T. Sherman, R. Stephens, M.W. Baseler, H.C. Lane, R.A. Lempicki, DAVID  
834 gene ID conversion tool, *Bioinformatics.* 2 (2008) 428–430.  
835 <https://doi.org/10.6026/97320630002428>.
- 836 [44] D.W. Huang, B.T. Sherman, R.A. Lempicki, Bioinformatics enrichment tools: paths toward the  
837 comprehensive functional analysis of large gene lists, *Nucleic Acids Res.* 37 (2009) 1–13.  
838 <https://doi.org/10.1093/nar/gkn923>.
- 839 [45] A.-A. Chassot, S.T. Bradford, A. Auguste, E.P. Gregoire, E. Pailhoux, D.G. de Rooij, A. Schedl,  
840 M.-C. Chaboissier, WNT4 and RSP01 together are required for cell proliferation in the early  
841 mouse gonad, *Development.* 139 (2012) 4461–4472. <https://doi.org/10.1242/dev.078972>.

- 842 [46] M. Kruithof-de Julio, M. Shibata, N. Desai, M. Reynon, M.V. Halili, Y.-P. Hu, S.M. Price, C.  
 843 Abate-Shen, M.M. Shen, Canonical Wnt signaling regulates Nkx3.1 expression and luminal  
 844 epithelial differentiation during prostate organogenesis, *Dev Dyn.* 242 (2013) 1160–1171.  
 845 <https://doi.org/10.1002/dvdy.24008>.
- 846 [47] X. Wang, M. Kruithof-de Julio, K.D. Economides, D. Walker, H. Yu, M.V. Halili, Y.-P. Hu, S.M.  
 847 Price, C. Abate-Shen, M.M. Shen, A luminal epithelial stem cell that is a cell of origin for prostate  
 848 cancer, *Nature.* 461 (2009) 495–500. <https://doi.org/10.1038/nature08361>.
- 849 [48] S.C. Baca, D. Prandi, M.S. Lawrence, J.M. Mosquera, A. Romanel, Y. Drier, K. Park, N.  
 850 Kitabayashi, T.Y. MacDonald, M. Ghandi, E. Van Allen, G.V. Kryukov, A. Sboner, J.-P.  
 851 Theurillat, T.D. Soong, E. Nickerson, D. Auclair, A. Tewari, H. Beltran, R.C. Onofrio, G. Boysen,  
 852 C. Guiducci, C.E. Barbieri, K. Cibulskis, A. Sivachenko, S.L. Carter, G. Saksena, D. Voet, A.H.  
 853 Ramos, W. Winckler, M. Cipicchio, K. Ardlie, P.W. Kantoff, M.F. Berger, S.B. Gabriel, T.R.  
 854 Golub, M. Meyerson, E.S. Lander, O. Elemento, G. Getz, F. Demichelis, M.A. Rubin, L.A.  
 855 Garraway, Punctuated evolution of prostate cancer genomes, *Cell.* 153 (2013) 666–677.  
 856 <https://doi.org/10.1016/j.cell.2013.03.021>.
- 857 [49] C.R. Bethel, D. Faith, X. Li, B. Guan, J.L. Hicks, F. Lan, R.B. Jenkins, C.J. Bieberich, A.M. De  
 858 Marzo, Decreased NKX3.1 protein expression in focal prostatic atrophy, prostatic intraepithelial  
 859 neoplasia, and adenocarcinoma: association with gleason score and chromosome 8p deletion,  
 860 *Cancer Res.* 66 (2006) 10683–10690. <https://doi.org/10.1158/0008-5472.CAN-06-0963>.
- 861 [50] M.J. Kim, R.D. Cardiff, N. Desai, W.A. Banach-Petrosky, R. Parsons, M.M. Shen, C. Abate-  
 862 Shen, Cooperativity of Nkx3.1 and Pten loss of function in a mouse model of prostate  
 863 carcinogenesis, *Proc Natl Acad Sci U S A.* 99 (2002) 2884–2889.  
 864 <https://doi.org/10.1073/pnas.042688999>.
- 865 [51] M.C. Markowski, C. Bowen, E.P. Gelmann, Inflammatory cytokines induce phosphorylation and  
 866 ubiquitination of prostate suppressor protein NKX3.1, *Cancer Res.* 68 (2008) 6896–6901.  
 867 <https://doi.org/10.1158/0008-5472.CAN-08-0578>.
- 868 [52] B.S. Taylor, N. Schultz, H. Hieronymus, A. Gopalan, Y. Xiao, B.S. Carver, V.K. Arora, P.  
 869 Kaushik, E. Cerami, B. Reva, Y. Antipin, N. Mitsiades, T. Landers, I. Dolgalev, J.E. Major, M.  
 870 Wilson, N.D. Socci, A.E. Lash, A. Heguy, J.A. Eastham, H.I. Scher, V.E. Reuter, P.T. Scardino,  
 871 C. Sander, C.L. Sawyers, W.L. Gerald, Integrative genomic profiling of human prostate cancer,  
 872 *Cancer Cell.* 18 (2010) 11–22. <https://doi.org/10.1016/j.ccr.2010.05.026>.
- 873 [53] A. Padmanabhan, V. Rao, A.M. De Marzo, C.J. Bieberich, Regulating NKX3.1 stability and  
 874 function: Post-translational modifications and structural determinants, *Prostate.* 76 (2016) 523–  
 875 533. <https://doi.org/10.1002/pros.23144>.
- 876 [54] E. Asatiani, W.-X. Huang, A. Wang, E. Rodriguez Ortner, L.R. Cavalli, B.R. Haddad, E.P.  
 877 Gelmann, Deletion, methylation, and expression of the NKX3.1 suppressor gene in primary  
 878 human prostate cancer, *Cancer Res.* 65 (2005) 1164–1173. <https://doi.org/10.1158/0008-5472.CAN-04-2688>.
- 880 [55] C. Bowen, L. Bubendorf, H.J. Voeller, R. Slack, N. Willi, G. Sauter, T.C. Gasser, P. Koivisto,  
 881 E.E. Lack, J. Kononen, O.P. Kallioniemi, E.P. Gelmann, Loss of NKX3.1 expression in human  
 882 prostate cancers correlates with tumor progression, *Cancer Res.* 60 (2000) 6111–6115.
- 883 [56] B. Gurel, T.Z. Ali, E.A. Montgomery, S. Begum, J. Hicks, M. Goggins, C.G. Eberhart, D.P. Clark,  
 884 C.J. Bieberich, J.I. Epstein, A.M. De Marzo, NKX3.1 as a marker of prostatic origin in metastatic  
 885 tumors, *Am J Surg Pathol.* 34 (2010) 1097–1105.  
 886 <https://doi.org/10.1097/PAS.0b013e3181e6cbf3>.
- 887 [57] J.C. Brenner, B. Ateeq, Y. Li, A.K. Yocum, Q. Cao, I.A. Asangani, S. Patel, X. Wang, H. Liang,  
 888 J. Yu, N. Palanisamy, J. Siddiqui, W. Yan, X. Cao, R. Mehra, A. Sabolch, V. Basrur, R.J.  
 889 Lonigro, J. Yang, S.A. Tomlins, C.A. Maher, K.S.J. Elenitoba-Johnson, M. Hussain, N.M.  
 890 Navone, K.J. Pienta, S. Varambally, F.Y. Feng, A.M. Chinnaiyan, Mechanistic rationale for  
 891 inhibition of poly(ADP-ribose) polymerase in ETS gene fusion-positive prostate cancer, *Cancer*  
 892 *Cell.* 19 (2011) 664–678. <https://doi.org/10.1016/j.ccr.2011.04.010>.
- 893 [58] P. Chatterjee, G.S. Choudhary, A. Sharma, K. Singh, W.D. Heston, J. Ciezki, E.A. Klein, A.  
 894 Almasan, PARP inhibition sensitizes to low dose-rate radiation TMPRSS2-ERG fusion gene-  
 895 expressing and PTEN-deficient prostate cancer cells, *PLoS One.* 8 (2013) e60408.  
 896 <https://doi.org/10.1371/journal.pone.0060408>.

- 897 [59] P. Chatterjee, G.S. Choudhary, T. Alswillah, X. Xiong, W.D. Heston, C. Magi-Galluzzi, J. Zhang,  
 898 E.A. Klein, A. Almasan, The TMPRSS2-ERG Gene Fusion Blocks XRCC4-Mediated  
 899 Nonhomologous End-Joining Repair and Radiosensitizes Prostate Cancer Cells to PARP  
 900 Inhibition, *Mol Cancer Ther.* 14 (2015) 1896–1906. <https://doi.org/10.1158/1535-7163.MCT-14-0865>.  
 901
- 902 [60] C. Bowen, E.P. Gelmann, NKX3.1 activates cellular response to DNA damage, *Cancer Res.*  
 903 70 (2010) 3089–3097. <https://doi.org/10.1158/0008-5472.CAN-09-3138>.  
 904
- 905 [61] C. Bowen, J.-H. Ju, J.-H. Lee, T.T. Paull, E.P. Gelmann, Functional activation of ATM by the  
 906 prostate cancer suppressor NKX3.1, *Cell Rep.* 4 (2013) 516–529.  
<https://doi.org/10.1016/j.celrep.2013.06.039>.  
 907
- 908 [62] X. Ouyang, T.L. DeWeese, W.G. Nelson, C. Abate-Shen, Loss-of-function of Nkx3.1 promotes  
 909 increased oxidative damage in prostate carcinogenesis, *Cancer Res.* 65 (2005) 6773–6779.  
<https://doi.org/10.1158/0008-5472.CAN-05-1948>.  
 910
- 911 [63] A. Papachristodoulou, A. Rodriguez-Calero, S. Panja, E. Margolskee, R.K. Virk, T.A. Milner,  
 912 L.P. Martina, J.Y. Kim, M. Di Bernardo, A.B. Williams, E.A. Maliza, J.M. Caputo, C. Haas, V.  
 913 Wang, G.J. De Castro, S. Wenske, H. Hibshoosh, J.M. McKiernan, M.M. Shen, M.A. Rubin, A.  
 914 Mitrofanova, A. Dutta, C. Abate-Shen, NKX3.1 Localization to Mitochondria Suppresses  
 915 Prostate Cancer Initiation, *Cancer Discov.* 11 (2021) 2316–2333. <https://doi.org/10.1158/2159-8290.CD-20-1765>.  
 916
- 917 [64] H. Zhang, T. Zheng, C.W. Chua, M. Shen, E.P. Gelmann, Nkx3.1 controls the DNA repair  
 918 response in the mouse prostate, *Prostate.* 76 (2016) 402–408.  
<https://doi.org/10.1002/pros.23131>.  
 919
- 920 [65] E. Elinav, R. Nowarski, C.A. Thaiss, B. Hu, C. Jin, R.A. Flavell, Inflammation-induced cancer:  
 921 crosstalk between tumours, immune cells and microorganisms, *Nat Rev Cancer.* 13 (2013)  
 922 759–771. <https://doi.org/10.1038/nrc3611>.  
 923
- 924 [66] A.M. Blee, Y. He, Y. Yang, Z. Ye, Y. Yan, Y. Pan, T. Ma, J. Dugdale, E. Kuehn, M. Kohli, R.  
 925 Jimenez, Y. Chen, W. Xu, L. Wang, H. Huang, TMPRSS2-ERG Controls Luminal Epithelial  
 926 Lineage and Antiandrogen Sensitivity in PTEN and TP53-Mutated Prostate Cancer, *Clin*  
 927 *Cancer Res.* 24 (2018) 4551–4565. <https://doi.org/10.1158/1078-0432.CCR-18-0653>.  
 928
- 929 [67] F. Li, Q. Yuan, W. Di, X. Xia, Z. Liu, N. Mao, L. Li, C. Li, J. He, Y. Li, W. Guo, X. Zhang, Y. Zhu,  
 930 R. Aji, S. Wang, X. Tong, H. Ji, P. Chi, B. Carver, Y. Wang, Y. Chen, D. Gao, ERG orchestrates  
 931 chromatin interactions to drive prostate cell fate reprogramming, *J Clin Invest.* 130 (2020)  
 932 5924–5941. <https://doi.org/10.1172/JCI137967>.  
 933
- 934 [68] D. Hanahan, R.A. Weinberg, Hallmarks of cancer: the next generation, *Cell.* 144 (2011) 646–  
 935 674. <https://doi.org/10.1016/j.cell.2011.02.013>.  
 936
- 937 [69] K. Ganapathy, S. Staklinski, M.F. Hasan, R. Ottman, T. Andl, A.E. Berglund, J.Y. Park, R.  
 938 Chakrabarti, Multifaceted Function of MicroRNA-299-3p Fosters an Antitumor Environment  
 939 Through Modulation of Androgen Receptor and VEGFA Signaling Pathways in Prostate  
 940 Cancer, *Sci Rep.* 10 (2020) 5167. <https://doi.org/10.1038/s41598-020-62038-3>.  
 941
- 942 [70] S. Ibaragi, N. Yoshioka, S. Li, M.G. Hu, S. Hirukawa, P.M. Sadow, G.-F. Hu, Neamine inhibits  
 943 prostate cancer growth by suppressing angiogenin-mediated rRNA transcription, *Clin Cancer*  
 944 *Res.* 15 (2009) 1981–1988. <https://doi.org/10.1158/1078-0432.CCR-08-2593>.  
 945
- 946 [71] S. Soker, M. Kaefer, M. Johnson, M. Klagsbrun, A. Atala, M.R. Freeman, Vascular endothelial  
 947 growth factor-mediated autocrine stimulation of prostate tumor cells coincides with progression  
 948 to a malignant phenotype, *Am J Pathol.* 159 (2001) 651–659. [https://doi.org/10.1016/S0002-9440\(10\)61736-1](https://doi.org/10.1016/S0002-9440(10)61736-1).  
 949
- 950 [72] W. Wang, X. Yang, J. Dai, Y. Lu, J. Zhang, E.T. Keller, Prostate cancer promotes a vicious  
 951 cycle of bone metastasis progression through inducing osteocytes to secrete GDF15 that  
 952 stimulates prostate cancer growth and invasion, *Oncogene.* 38 (2019) 4540–4559.  
<https://doi.org/10.1038/s41388-019-0736-3>.  
 953
- 954 [73] H.-P. Yao, Y.-Q. Zhou, R. Zhang, M.-H. Wang, MSP-RON signalling in cancer: pathogenesis  
 955 and therapeutic potential, *Nat Rev Cancer.* 13 (2013) 466–481.  
<https://doi.org/10.1038/nrc3545>.  
 956
- 957 [74] C. Abate-Shen, M.M. Shen, E. Gelmann, Integrating differentiation and cancer: the Nkx3.1  
 958 homeobox gene in prostate organogenesis and carcinogenesis, *Differentiation.* 76 (2008) 717–  
 959 727. <https://doi.org/10.1111/j.1432-0436.2008.00292.x>.

- 953 [75] Cancer Genome Atlas Research Network, The Molecular Taxonomy of Primary Prostate  
954 Cancer, *Cell*. 163 (2015) 1011–1025. <https://doi.org/10.1016/j.cell.2015.10.025>.
- 955 [76] S.M.G. Espiritu, L.Y. Liu, Y. Rubanova, V. Bhandari, E.M. Holgersen, L.M. Szyca, N.S. Fox,  
956 M.L.K. Chua, T.N. Yamaguchi, L.E. Heisler, J. Livingstone, J. Wintersinger, F. Yousif, E.  
957 Lalonde, A. Rouette, A. Salcedo, K.E. Houlahan, C.H. Li, V. Huang, M. Fraser, T. van der  
958 Kwast, Q.D. Morris, R.G. Bristow, P.C. Boutros, The Evolutionary Landscape of Localized  
959 Prostate Cancers Drives Clinical Aggression, *Cell*. 173 (2018) 1003-1013.e15.  
960 <https://doi.org/10.1016/j.cell.2018.03.029>.
- 961 [77] M.J. Kim, R. Bhatia-Gaur, W.A. Banach-Petrosky, N. Desai, Y. Wang, S.W. Hayward, G.R.  
962 Cunha, R.D. Cardiff, M.M. Shen, C. Abate-Shen, Nkx3.1 mutant mice recapitulate early stages  
963 of prostate carcinogenesis, *Cancer Res*. 62 (2002) 2999–3004.
- 964 [78] R. Bhatia-Gaur, A.A. Donjacour, P.J. Sciavolino, M. Kim, N. Desai, P. Young, C.R. Norton, T.  
965 Gridley, R.D. Cardiff, G.R. Cunha, C. Abate-Shen, M.M. Shen, Roles for Nkx3.1 in prostate  
966 development and cancer, *Genes Dev*. 13 (1999) 966–977.  
967 <https://doi.org/10.1101/gad.13.8.966>.
- 968 [79] J.A. Magee, S.A. Abdulkadir, J. Milbrandt, Haploinsufficiency at the Nkx3.1 locus. A paradigm  
969 for stochastic, dosage-sensitive gene regulation during tumor initiation, *Cancer Cell*. 3 (2003)  
970 273–283. [https://doi.org/10.1016/s1535-6108\(03\)00047-3](https://doi.org/10.1016/s1535-6108(03)00047-3).
- 971 [80] F. Talos, A. Mitrofanova, S.K. Bergren, A. Califano, M.M. Shen, A computational systems  
972 approach identifies synergistic specification genes that facilitate lineage conversion to prostate  
973 tissue, *Nat Commun*. 8 (2017) 14662. <https://doi.org/10.1038/ncomms14662>.
- 974 [81] C.-C. Yang, A. Chung, C.-Y. Ku, L.M. Brill, R. Williams, D.A. Wolf, Systems analysis of the  
975 prostate tumor suppressor NKX3.1 supports roles in DNA repair and luminal cell differentiation,  
976 *F1000Res*. 3 (2014) 115. <https://doi.org/10.12688/f1000research.3818.2>.
- 977 [82] S. Irshad, C. Abate-Shen, Modeling prostate cancer in mice: something old, something new,  
978 something premalignant, something metastatic, *Cancer Metastasis Rev*. 32 (2013) 109–122.  
979 <https://doi.org/10.1007/s10555-012-9409-1>.
- 980 [83] C. Le Magnen, R.K. Virk, A. Dutta, J.Y. Kim, S. Panja, Z.A. Lopez-Bujanda, A. Califano, C.G.  
981 Drake, A. Mitrofanova, C. Abate-Shen, Cooperation of loss of NKX3.1 and inflammation in  
982 prostate cancer initiation, *Dis Model Mech*. 11 (2018) dmm035139.  
983 <https://doi.org/10.1242/dmm.035139>.
- 984 [84] R. Thangapazham, F. Saenz, S. Katta, A.A. Mohamed, S.-H. Tan, G. Petrovics, S. Srivastava,  
985 A. Dobi, Loss of the NKX3.1 tumorsuppressor promotes the TMPRSS2-ERG fusion gene  
986 expression in prostate cancer, *BMC Cancer*. 14 (2014) 16. [https://doi.org/10.1186/1471-2407-](https://doi.org/10.1186/1471-2407-14-16)  
987 14-16.
- 988 [85] C. Bowen, T. Zheng, E.P. Gelmann, NKX3.1 Suppresses TMPRSS2-ERG Gene  
989 Rearrangement and Mediates Repair of Androgen Receptor-Induced DNA Damage, *Cancer*  
990 *Res*. 75 (2015) 2686–2698. <https://doi.org/10.1158/0008-5472.CAN-14-3387>.
- 991 [86] J. Lapointe, C. Li, C.P. Giacomini, K. Salari, S. Huang, P. Wang, M. Ferrari, T. Hernandez-  
992 Boussard, J.D. Brooks, J.R. Pollack, Genomic profiling reveals alternative genetic pathways of  
993 prostate tumorigenesis, *Cancer Res*. 67 (2007) 8504–8510. [https://doi.org/10.1158/0008-](https://doi.org/10.1158/0008-5472.CAN-07-0673)  
994 5472.CAN-07-0673.
- 995 [87] P. Kunderfranco, M. Mello-Grand, R. Cangemi, S. Pellini, A. Mensah, V. Albertini, A. Malek, G.  
996 Chiorino, C.V. Catapano, G.M. Carbone, ETS transcription factors control transcription of EZH2  
997 and epigenetic silencing of the tumor suppressor gene Nkx3.1 in prostate cancer, *PLoS One*.  
998 5 (2010) e10547. <https://doi.org/10.1371/journal.pone.0010547>.
- 999 [88] Z. Hong, W. Zhang, D. Ding, Z. Huang, Y. Yan, W. Cao, Y. Pan, X. Hou, S.J. Weroha, R.J.  
1000 Karnes, D. Wang, Q. Wu, D. Wu, H. Huang, DNA Damage Promotes TMPRSS2-ERG  
1001 Oncoprotein Destruction and Prostate Cancer Suppression via Signaling Converged by GSK3 $\beta$   
1002 and WEE1, *Mol Cell*. 79 (2020) 1008-1023.e4. <https://doi.org/10.1016/j.molcel.2020.07.028>.
- 1003



## 1 **Figure Legends**

2

### 3 **Figure 1. Establishing mouse Prostate Organoids Culture**

4 A. Scheme showing prostate organoids derivation from wild type mouse adult prostate tissue.

5 B. Organoid culture growth within ECM-like domes. Scale bar: 200  $\mu\text{m}$ .

6 C. Immunofluorescent analysis of basal (Krt 5) and luminal (Krt 8; Ar) markers in mouse prostate  
7 organoids (left panels) and adult prostate tissue (right panels). DAPI was used for nuclear staining.  
8 Lower panels show inset magnifications of specified area. Scale bars: 50  $\mu\text{m}$  upper panels; 10  $\mu\text{m}$   
9 lower panels.

10 D. Western blot analysis of Ar in mouse prostate organoids with or without dihydrotestosterone  
11 (DHT).

12 E. Expression levels of Ar target genes in mouse prostate organoids cultured with or without DHT.  
13 Statistical analyses were performed on at least  $n=3$  independent biological replicates. \*= p-value  
14  $<0.05$ ; \*\*= p-value  $<0.01$ .

15

### 16 **Figure 2. Characterization of mPrOs-*ERG*<sub>M40</sub>**

17 A. Phenotypic analysis of mPrOs-WT and mPrOs-*ERG*<sub>M40</sub> treated for 96 hours with doxycycline  
18 (doxy) or left untreated (mock). Scale bars: 200  $\mu\text{m}$ .

19 B. *ERG* expression in mPrOs. cDNA from VCAP cell line was used as positive control.

20 C. Immunoblot with *ERG*-specific antibody of protein extracts from mPrOs-WT and mPrOs-*ERG*<sub>M40</sub>  
21 treated with doxycycline for 96 hours or left untreated. Gapdh was used as loading control.

22 D. RT-qPCR analysis of known *ERG*-targeted genes in mPrOs-*ERG*<sub>M40</sub> after treatment with or  
23 without doxycycline for 96 hours. mPrOs-WT were used as reference.

24 E. Immunofluorescence analysis of *ERG*, Krt 8 and Krt 5 in mPrOs-WT and mPrOs-*ERG*<sub>M40</sub> treated  
25 with doxycycline for 96 hours (doxy) or left untreated (mock). DAPI was used for nuclear staining.  
26 Scale bars: 50  $\mu\text{m}$ .

27 F. Immunoblot analysis of Krt 8 and Krt 5 expression in mPrOs-WT and mPrOs-*ERG*<sub>M40</sub> treated with  
28 doxycycline for 96 hours or left untreated. Gapdh was used as loading control.

29 G. RT-qPCR analysis of *Krt 5* and *Krt 8* expression in mPrOs-*ERG*<sub>M40</sub> treated with doxycycline (doxy)  
30 for 96 hours or left untreated (mock).

31 H. Immunofluorescence analysis of *ERG* and Ki67 expression mPrOs-WT and mPrOs-*ERG*<sub>M40</sub>  
32 treated with doxycycline for 96 hours or left untreated. DAPI was used for nuclear staining. Scale  
33 bars: 50  $\mu\text{m}$ .

34 I. Percentage of Ki67+ cells in mPrOs-WT and mPrOs-*ERG*<sub>M40</sub> treated with doxycycline for 96 hours  
35 or left untreated. Quantification was performed on sections of  $n=10$  organoids per condition (WT  
36 mock = 1.396; WT doxy = 1.181; *ERG*<sub>M40</sub> = 1.380; *ERG*<sub>M40</sub> doxy = 1.345 total cells counted).

37 J. Analysis of cell cycle progression of mPrOs-WT and mPrOs-ERG<sub>M40</sub> treated with doxycycline for  
 38 96 hours or left untreated. Histogram shows the quantification of the FACS analysis.  
 39 K. Phenotypic analysis of mPrOs-WT and mPrOs-ERG<sub>M40</sub> cultured with Egf-free medium for up to  
 40 two weeks. Doxycycline was maintained throughout the duration of the experiment. Fluorescent  
 41 images were acquired following 1 hour incubation with 5  $\mu$ M calcein. Scale bars: 200  $\mu$ m.  
 42 Statistical analyses were performed on at least n=3 independent biological replicates. \*= p-value  
 43 <0.05; \*\*= p-value <0.01; \*\*\*= p-value <0.001.

44

### 45 **Figure 3. Mass spectrometry analysis of secreted proteins**

46 A. Schematic representation of Click-it chemistry coupled Mass Spectrometry approach.  
 47 B. Venn diagram showing the number of secreted proteins identified from mPrOs-WT (n=4).  
 48 C. Histogram showing the top 10 enriched pathways identified by STRING (V 11.0).  
 49 D. Protein-Protein interaction network obtained with STRING (V 11.0) generated starting from the  
 50 secreted proteins included in the pathway "Innate Immune System", highlighted in C.  
 51 E. mPrOs-WT and mPrOs-ERG<sub>M40</sub> organoids treated with doxycycline for 96 hours or left untreated,  
 52 labelled O/N with AHA. Scale bar: 200  $\mu$ m.  
 53 F. Venn diagrams showing the degree of shared and unique proteins in the four conditions described  
 54 in E. Identified proteins were associated to a specific condition if identified with at least 2 "Unique  
 55 peptides" in at least 3 biological replicates (n=4).  
 56 G. Heatmap showing LFQ intensity values for each protein in each analyzed sample.  
 57 H. Volcano plot showing proteins differentially secreted by mPrOs-ERG<sub>M40</sub> treated with doxycycline  
 58 or left untreated. Colored spots are associated to proteins of interest.  
 59 I. Volcano plot comparing mPrOs-WT treated with doxycycline or left. Colored spots code as in H.  
 60 J. Expression analysis of the genes encoding the five most deregulated proteins in mPrOs-ERG<sub>M40</sub>.  
 61 Statistical analyses were performed on at least n=3 independent biological replicates. \*= p-value  
 62 <0.01.

63

### 64 **Figure 4. ERG<sub>M40</sub> inhibition of canonical Wnt pathway**

65 A. Immunoblot analysis of cytosolic and nuclear levels of  $\beta$ -Catenin in mPrOs-ERG<sub>M40</sub> treated with  
 66 doxycycline for 96 hours or left untreated.  
 67 B. RT-qPCR analysis of canonical Wnt pathway targeted genes in mPrOs described in A.  
 68 C. Immunoblot analysis of cytosolic and nuclear  $\beta$ -Catenin in mPrOs-ERG<sub>M40</sub> cultured without Rspo1  
 69 and treated with doxycycline for 96 hours or left untreated.  
 70 D. RT-qPCR analysis of canonical Wnt pathway targeted genes in mPrOs described in C.  
 71 E. Immunofluorescence analysis for  $\beta$ -Catenin (green) and Krt8 (red) in mPrOs-ERG<sub>M40</sub> treated with  
 72 doxycycline for 96 hours or left untreated, cultured in presence (ENRAD) or absence (EN-AD) of  
 73 Rspo1. (Scale bar: 10  $\mu$ m).

74 **Figure 5. *ERG<sub>M40</sub>* dependent mechanisms of genomic instability**

75 A. Nkx3.1 expression in mPrOs-WT cultured with or without Rspo1 (left), in mPrOs-*ERG<sub>M40</sub>* cultured  
76 with or without doxycycline (middle), and in mPrOs-*ERG<sub>M40</sub>* treated with doxycycline for 96 hours or  
77 left untreated and cultured without Rspo1 (right). T-test, \*= p value <0.05; \*\*= p-value <0.01; \*\*\*= p-  
78 value <0.001.

79 B. Immunoblot analysis of Nkx3.1 in wild type and *ERG<sub>M40</sub>* mPrOs cultured with or without Rspo1.  
80 mPrOs-*ERG<sub>M40</sub>* were treated with doxycycline for 96 hours or left untreated.

81 C. Immunoblot analysis of cytosolic and nuclear levels of Nkx3.1 in mPrOs-*ERG<sub>M40</sub>* treated with  
82 doxycycline for 96 hours or left untreated and cultured without Rspo1.

83 D. Immunoblot analysis of Nkx3.1 and *ERG<sub>M40</sub>* in mPrOs-*ERG<sub>M40</sub>* induced with doxycycline for 96  
84 hours cultured in presence or not of Rspo1 and treated or not with the proteasome inhibitor  
85 Bortezomib (5  $\mu$ M, 6 and 12 hours).

86 E. Comet assay of mPrOs-*ERG<sub>M40</sub>* induced or not with doxycycline (96 hours) and cultured in the  
87 presence or not of Rspo1. (n >100 comets analysed per condition). Wilcoxon test, \*= p value <0.05;  
88 \*\*\*= p-value <0.001.

89 F. Immunoblot analysis of DSBs markers  $\gamma$ H2ax, p-53bp1, and p-Atm in mPrOs-*ERG<sub>M40</sub>* induced or  
90 not with doxycycline for 96 hours cultured in presence or not of Rspo1 and treated or not with the  
91 Gsk3 $\beta$  inhibitor CHIR99021 (5  $\mu$ M, 6 days).

92

93 **Figure 6. *mPrOs* extracellular signals modify the molecular profile of M1 macrophage**

94 A. Schematic representation of secreted proteins isolated in the screening with known functions in  
95 macrophages biology.

96 B. Immunolocalization of CD68+ macrophages in *ERG*+ human high-grade prostatic intraepithelial  
97 neoplasia (HGPIN). Staining was performed on serial sections of paraffin embedded samples. Scale  
98 bar: 10  $\mu$ m

99 C. Schematic representation of the experimental workflow.

100 D-E. RT-qPCR analysis of genes characterizing M1 (*Il1b*, *Tnf $\alpha$* , *iNos*; D) or M2 (*Arg1*, *Chil3*; E)  
101 polarized macrophages conditioned (1:1) with the supernatants of mPrOs-WT and mPrOs-*ERG<sub>M40</sub>*  
102 treated or not with doxycycline for 96 hours. Unconditioned organoid medium was used as control.  
103 Statistical analyses were performed on at least n=3 independent biological replicates. \*= p value  
104 <0.05; \*\*= p-value <0.01; \*\*\*= p-value <0.001.

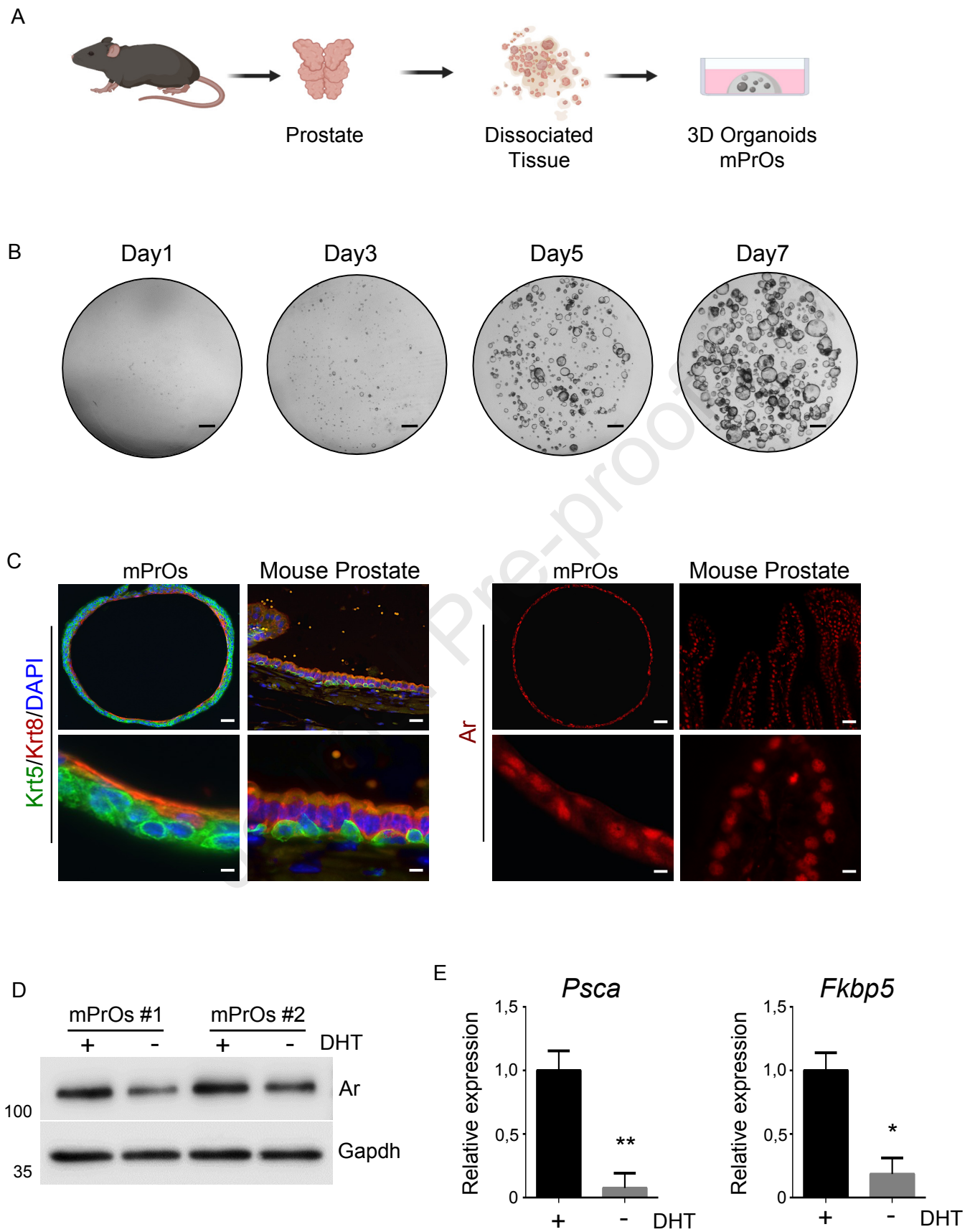
105

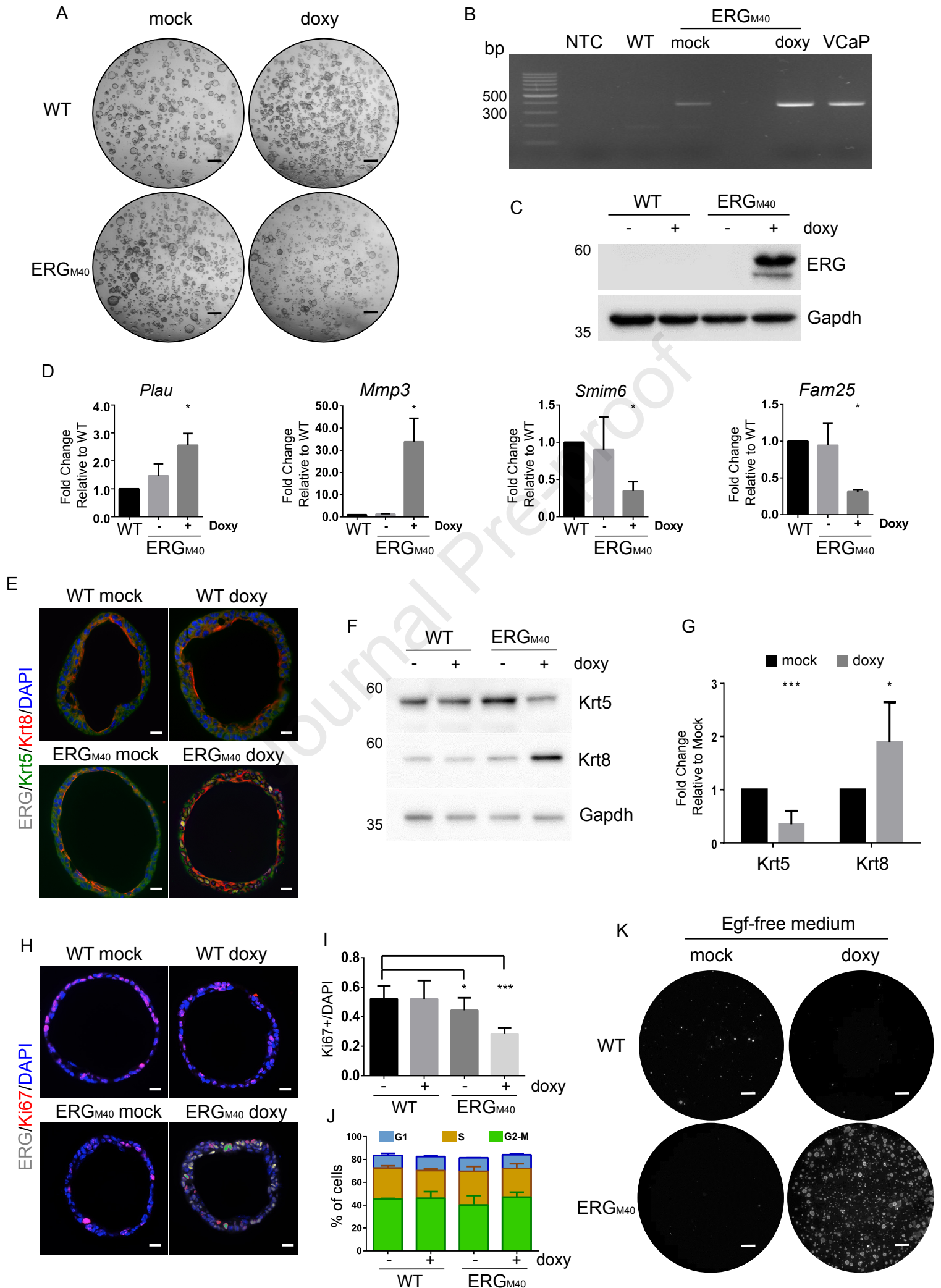
106 **Figure 7. Model of the molecular mechanisms primed by *ERG* to undermine cellular  
107 homeostasis and genome stability of adult prostate progenitors**

108

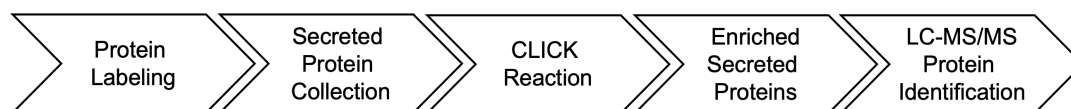
109

110

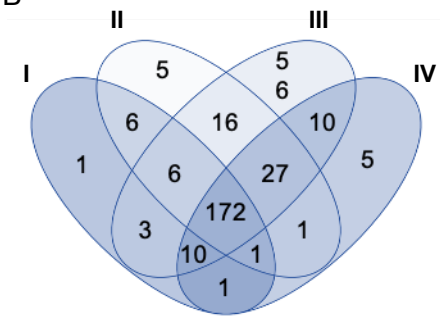




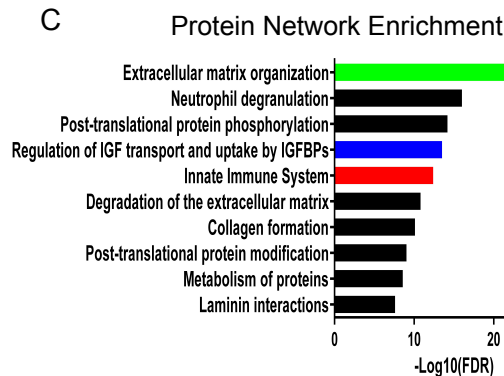
A



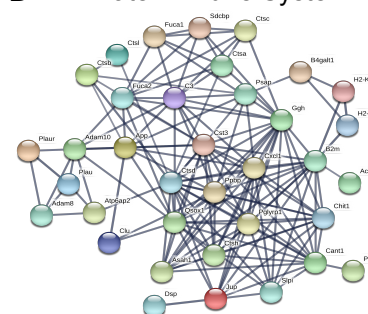
B



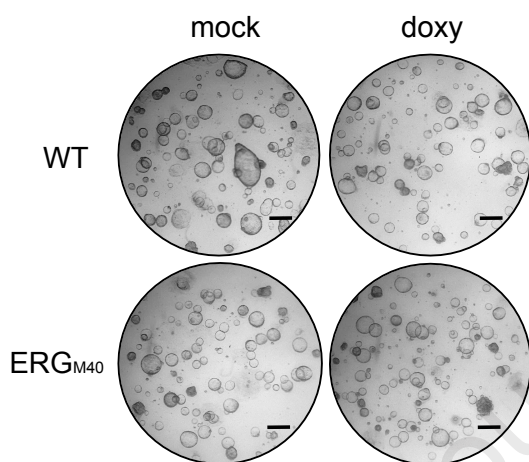
C



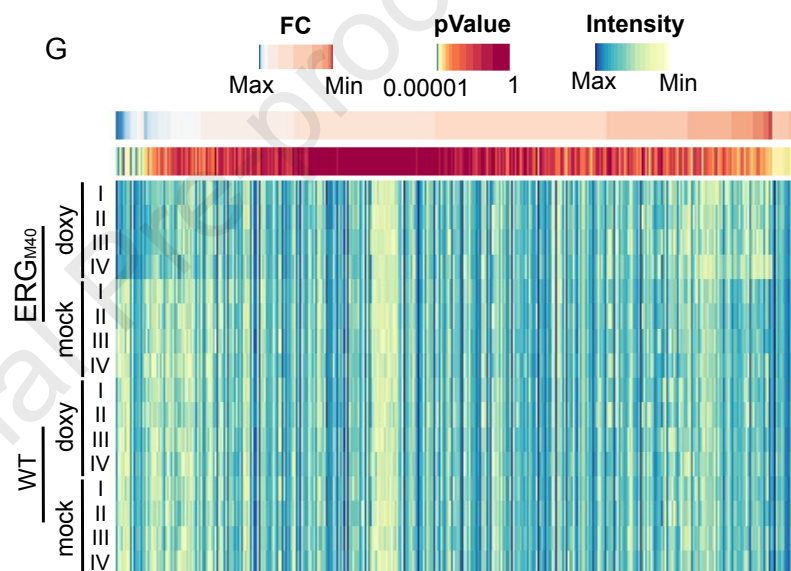
D



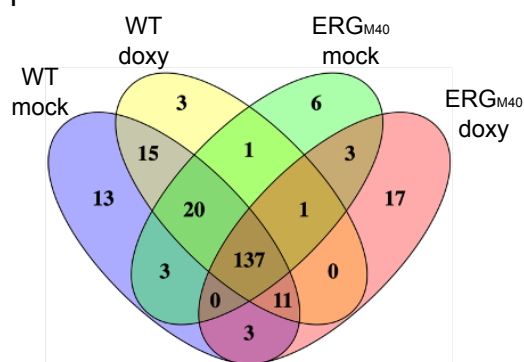
E



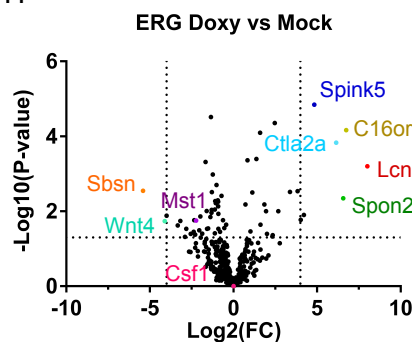
G



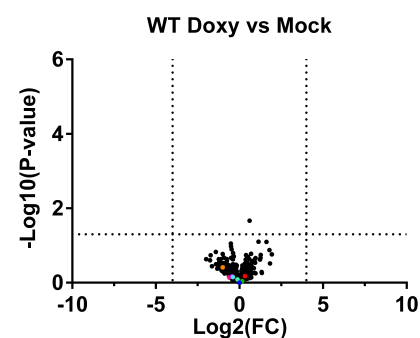
F



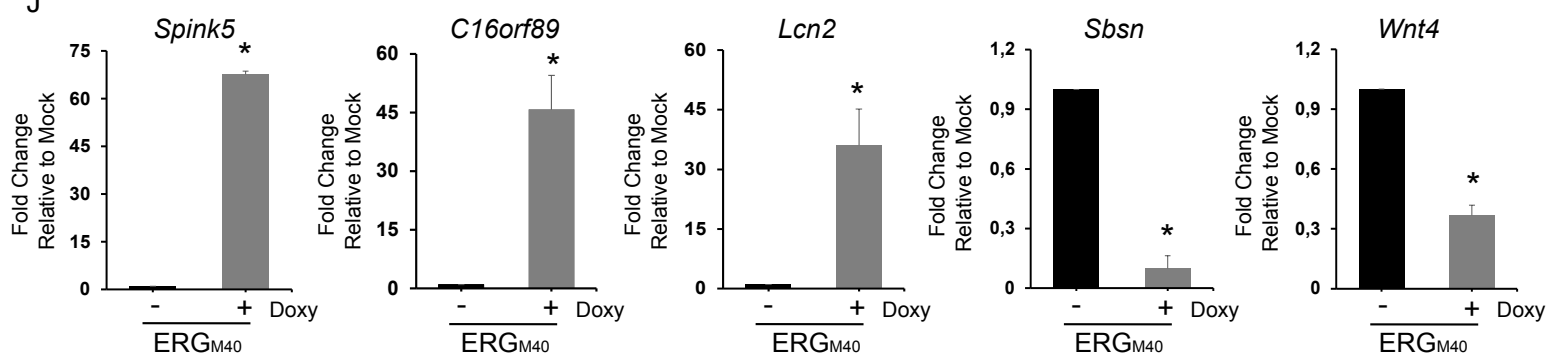
H

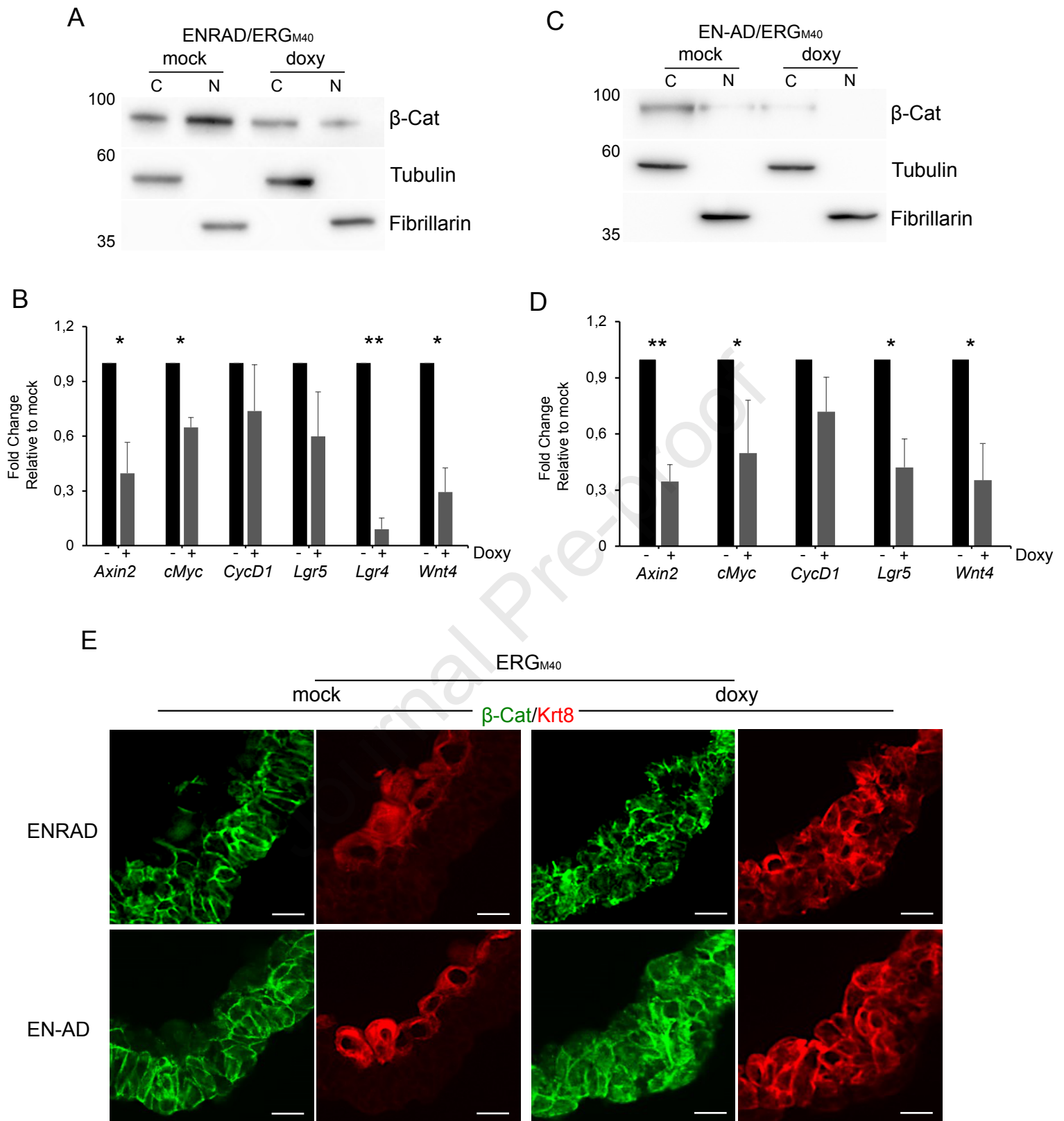


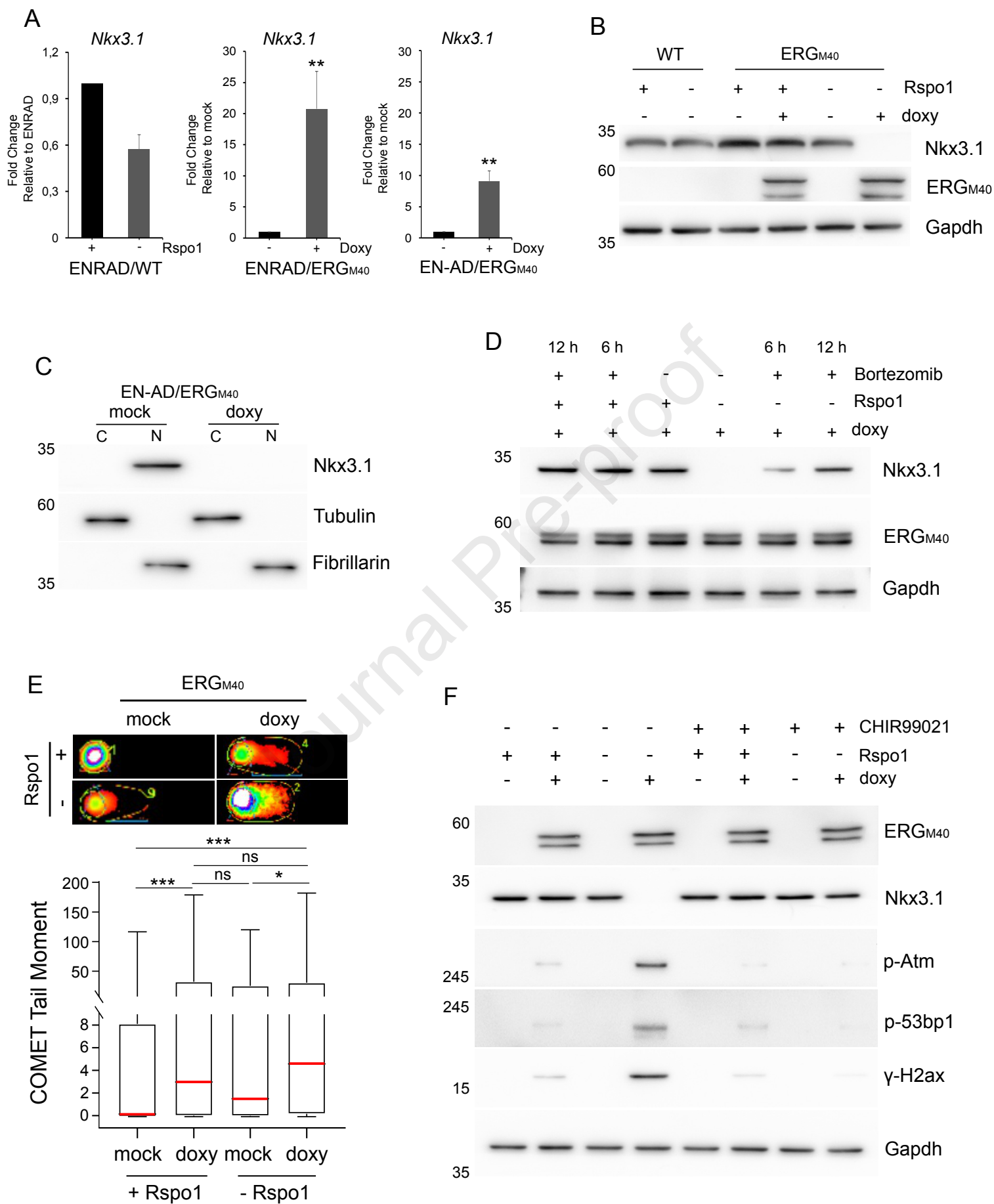
I



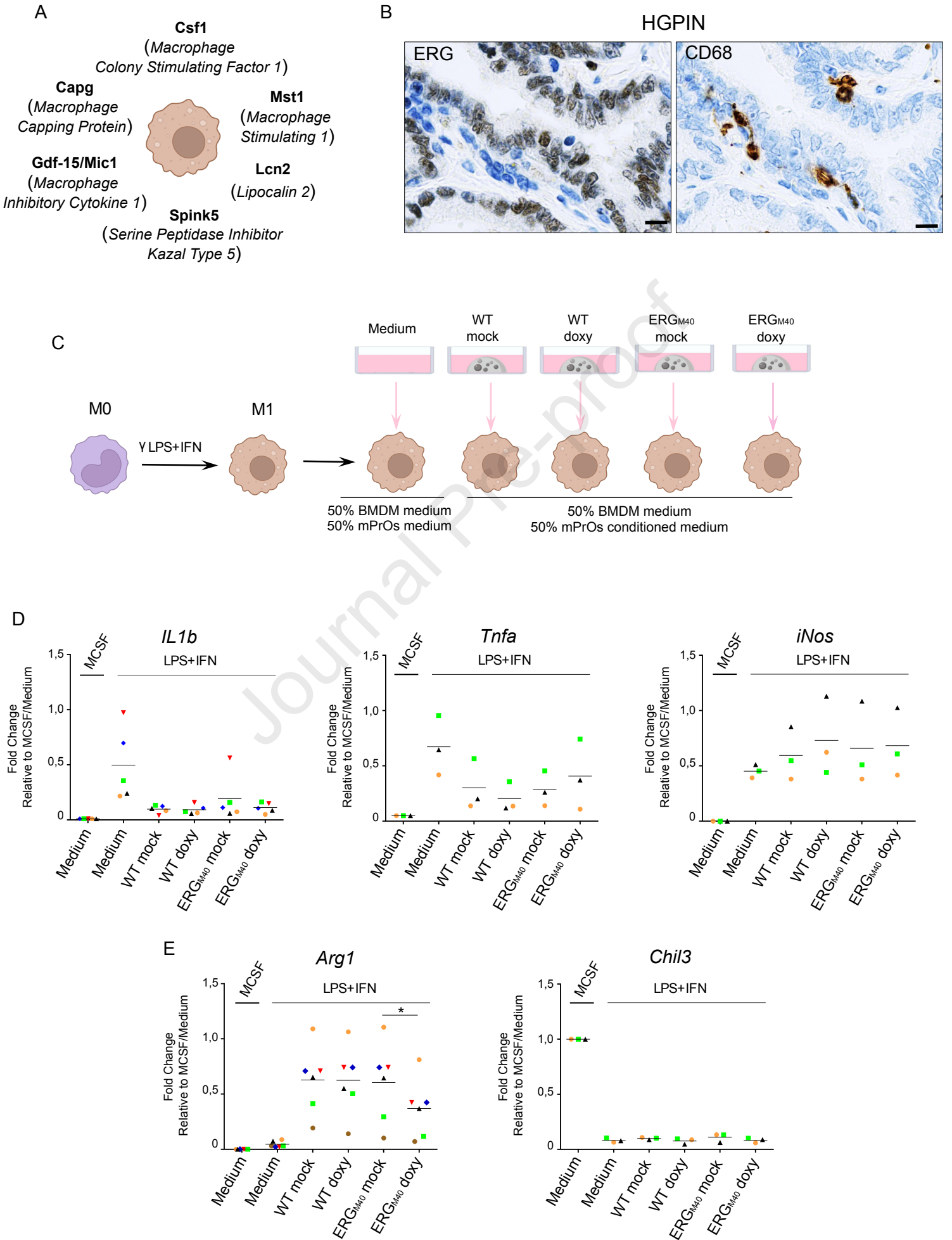
J

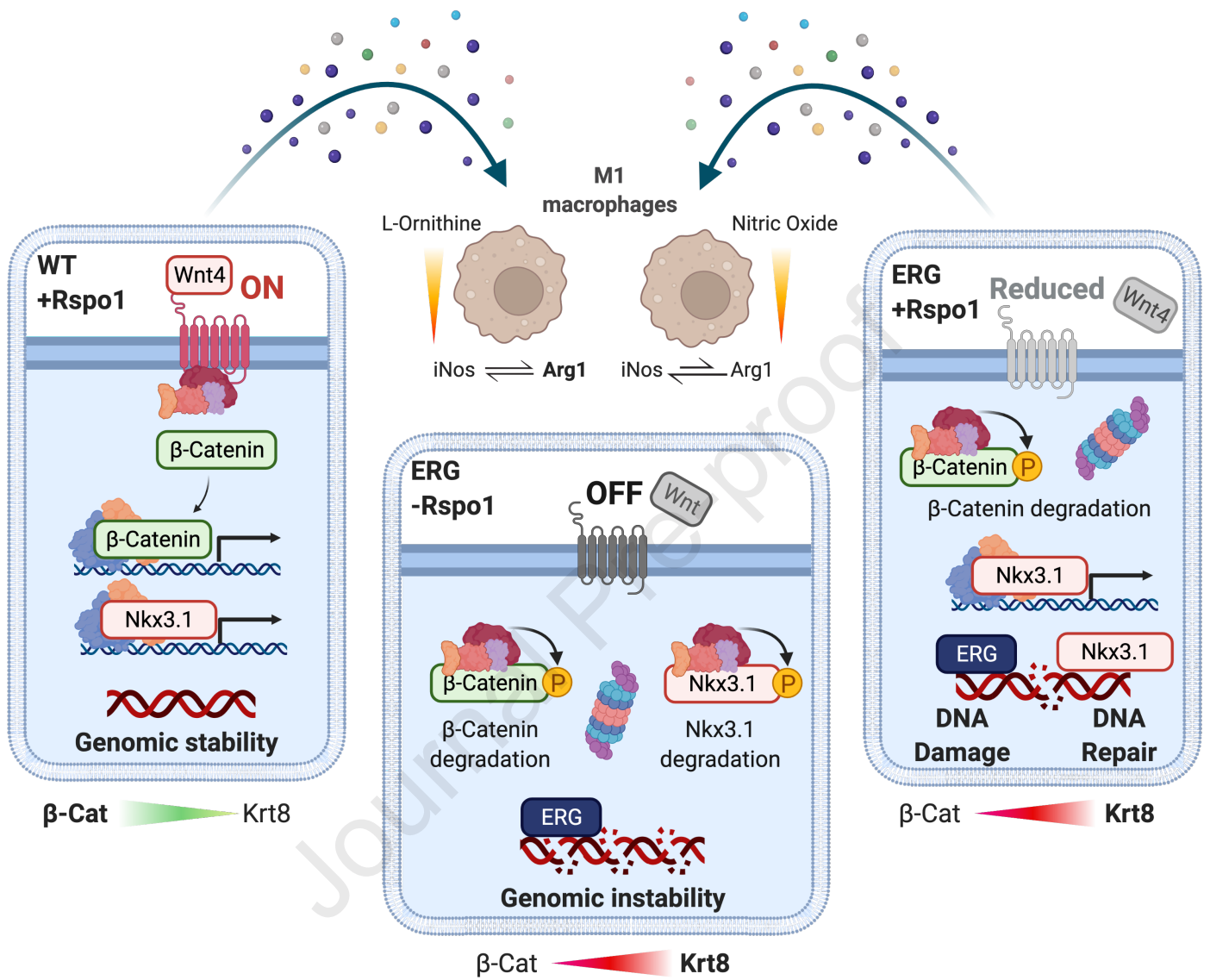












## Highlights

- Expression of ERG<sub>M40</sub> in mouse prostate organoids promotes their survival and growth in the absence of Egf.
- ERG<sub>M40</sub> alters the extracellular signaling network of mouse prostate organoids.
- Canonical Wnt pathway is substantially reduced in ERG+ prostate organoids due to decreased autocrine signaling of Wnt4.
- Gsk3b promotes Nkx3.1 proteolysis and, in turn, accumulation of double strand breaks in ERG+ prostate organoids.
- Paracrine signaling of ERG+ prostate organoids modulates *Arginase 1* expression in M1-polarized macrophages.

**Declaration of interests**

The authors declare that they have no known competing financial interests or personal relationships that could have appeared to influence the work reported in this paper.

The authors declare the following financial interests/personal relationships which may be considered as potential competing interests:

Journal Pre-proof